TOPICAL REVIEW • OPEN ACCESS

One (photon), two(-dimensional crystals), a lot (of potential): a quick snapshot of a rapidly evolving field

To cite this article: Salvatore Cianci *et al* 2024 *Nano Futures* **8** 012001

IOP Publishing Nano Futures 8 (2024) 012001 https://doi.org/10.1088/2399-1984/ad285b

NANO FUTURES

TOPICAL REVIEW

One (photon), two(-dimensional crystals), a lot (of potential): a quick snapshot of a rapidly evolving field

Salvatore Cianci, Elena Blundo and Marco Felici*

Physics Department, Sapienza University of Rome, Piazzale Aldo Moro, 5, Rome 00185, Italy
* Author to whom any correspondence should be addressed.

E-mail: marco.felici@uniroma1.it

OPEN ACCESS

RECEIVED
3 August 2023

REVISED
24 October 2023

ACCEPTED FOR PUBLICATION
12 February 2024

PUBLISHED
22 February 2024

Keywords: two-dimensional materials, quantum emitters, transition metal dichalcogenides, hexagonal boron nitride, quantum technologies

Abstract

We present a concise overview of the state of affairs in the development of single-photon sources based on two-dimensional (2D) crystals, focusing in particular on transition-metal dichalcogenides and hexagonal boron nitride. We briefly discuss the current level of advancement (*i*) in our understanding of the microscopic origin of the quantum emitters (QEs) identified in these two material systems, and (*ii*) in the characterisation of the optical properties of these emitters; then, we survey the main methods developed to enable the dynamic control of the QEs' emission energy. Finally, we summarise the main results stemming from the coupling of QEs embedded in 2D materials with photonic and plasmonic structures.

1. Introduction

Bringing quantum technologies from the lab to our everyday lives will require the engineering and implementation of devices that can meet the rigorous criteria set by mass applications. Of course, the availability of non-classical light sources emitting indistinguishable photons on demand will be of the utmost importance, together with the achievement of a high source efficiency and single-photon purity. As quantum devices inch closer to making the final leap towards the consumer market, however, a few, initially overlooked requirements are coming to the forefront: indeed, commercially viable single photon sources should be produced using manufacturing methods that are cheap, reliable, reproducible, and, preferably, compatible with current photonic integration technologies.

Epitaxial quantum dots (QDs) based on III–V materials are widely regarded as a very promising system within this field: due to the remarkable progresses made in the last decade [1–3], indeed, they feature nearly deterministic photon emission, with high efficiency and near-unity indistinguishability. Consequently, III–V QDs are, up to now, the only system that has been exploited commercially (see, e.g. http://quandela.com/ and https://sparrowquantum.com/). On the downside, self-assembled QDs notoriously suffer from stochastic site formation. This problem can only be partially mitigated using sophisticated approaches which, however, yield a lower optical quality of the QDs. Among these approaches, we would like to mention the use of lithographically patterned substrates—which leads to the formation of site-controlled pyramidal QDs by metallorganic vapour epitaxy [4] or the fabrication of site-controlled QDs through the exploitation of the effects of spatially controlled H irradiation [5] or removal [6] in dilute nitride semiconductors. In addition, established methods to enhance the QD emission rate and extraction efficiency rely on the spatial and spectral coupling to engineered photonic structures. While single devices fabricated with this method can feature ∼99% indistinguishability and extraction efficiencies up to ∼70% [7], all current approaches to fabricate such sources demand for manually selecting the QD emitters and/or the full devices [8–10], hindering scalability and dramatically increasing production time and costs. The combination of manual selection with the stochastic nature of the QD growth processes makes it a superior challenge to produce large numbers of identical sources of single (and, ideally, indistinguishable) photons, as required for quantum information science and technology. Moreover, the reliance of today's commercially available single-photon sources on III–V materials—and on InGaAs, in particular—is inextricably and inherently

entangled to the high fabrication costs typical for this platform. Indeed, the price for InGaAs-based devices commonly exceeds various tens of thousands of euros/dollars per single photon source, due both to the high costs of epitaxial growth techniques—crucial for achieving state-of-the-art material quality—and to the low supply potential of gallium and indium [11]. The latter point also raises questions about the long-term sustainability of a technological ecosystem entirely based on III–V materials.

Within this context, the quantum emitters (QEs) embedded in two-dimensional (2D) materials, e.g. in transition-metal dichalcogenides (TMDCs) and in hexagonal boron nitride (hBN), have the potential to successfully challenge the status quo. Both TMDCs and hBN belong to the vast family of layered semiconductors, wherein stacks of individual crystal layers—or monolayers (MLs)—characterised by strong in-plane covalent bonds, are held together, in the vertical direction, by much weaker [12] van der Waals forces. As it is well known, research interest around these materials skyrocketed following the successful isolation of atomically thin crystals of *graphene*, by simple mechanical exfoliation of graphite [13]. The application of the same method to a wide variety of materials, including TMDCs and hBN but also transition-metal chalcogenides [14] and layered metal-halide perovskites [15], has led to nearly two decades of uninterrupted scientific discoveries, which would be too long to even summarise here. What is most important, within the context of this work, is the fact that thin layers of TMDCs and hBN consistently display the ability to host bright single-photon sources [16–22], ranging in energy from the telecom window ($MoTe_2$, see [23]) to the visible range (hBN [20]). The costs of these sources are surprisingly modest, as $\sim$500 euros are currently sufficient to purchase a bulk specimen that can be used to fabricate hundreds of thin-layer flakes that, in turn, can each host hundreds of QEs. Costs aside, these thin flakes, when compared to 3D bulk crystals hosting QEs, feature a lack of internal reflection, leading to an increased light extraction efficiency, while their all-surface nature allows for the external manipulation of the emitters' properties. In addition, 2D MLs can be easily transferred on any substrate—including silicon-based photonic structures—thus ensuring significant advantages in terms of optical losses, manufacturing costs, and compatibility with CMOS electronics [24].

Moreover, 2D materials are particularly well-suited for the implementation of advanced strain engineering protocols. The introduction of controlled amounts of strain in the material indeed represents a well-established method for tuning the electronic properties of semiconductors. In conventional semiconductors, however, the amount of strain that can be introduced is traditionally fixed by the fabrication process [25]. While there has recently been significant progress in the development of methods to apply reconfigurable stresses to these materials, the maximal amount of strain that can be introduced in conventional semiconductors is typically capped at $\sim$1% by their elastic limit. These limitations can be greatly exceeded in the case of 2D materials, wherein sizeable, variable stresses can be easily applied. The reduced dimensionality in one direction—due to the weak van der Waals forces, by which the isolation of atomically thin, dangling bonds-free layers is made possible—allows for a greater deformation of the crystal. This feature, together with the reduced risk of fractures by virtue of the strong in-plane covalent bonds, leads to the possibility of introducing very large isotropic or anisotropic strains (total strains up to 10%–20%), thus tuning the electronic properties of these materials controllably over a very broad range [26–32]. As discussed in the following section, strain plays also an important role for the observation of the single-photon sources hosted by TMDCs [16, 18], which can be purposefully induced by localised, site-controlled stressors [33].

In the following two sections, the main features of TMDC- and hBN-based single-photon sources will be described; then, we will discuss the current state of the art with respect to the integration of these sources with photonic structures. Finally, we will conclude, providing our vision of the main breakthroughs to be expected—and of the most likely upcoming challenges to be faced—in this bustling research field.

2. TMDCs

TMDCs are layered materials whose single layer is comprised of a three-layer substructure MX_2, wherein a hexagonal lattice of transition metal atoms (M) is sandwiched between two other hexagonal lattice structures of chalcogen atoms (X). Semiconducting TMDCs, *e.g.* WS_2, WSe_2, MoS_2, $MoSe_2$, and $MoTe_2$, display a peculiar thickness-dependent indirect-to-direct bandgap transition [34–36]. Indeed, TMDCs in their bulk form feature an indirect bandgap and are, therefore, poor light emitters, since the radiative recombination of the electrons promoted in the conduction band with the holes left behind in the valence band requires the contribution of a phonon to conserve momentum. In TMDC MLs, however, the conduction- and valence-band edges can both be found at the K points of the Brillouin zone, thus making the transition direct and dramatically boosting the light-emission efficiency of these materials. The photoluminescence (PL) spectra of TMDC MLs are characterised by the presence of bright, prominent peaks related to *excitonic complexes* [37]. The reduced dimensionality of TMDC MLs leads to an increase in the exciton binding energy [38], making these quasiparticles robust to thermal excitations, and emitting even at room temperature (RT).

Moreover, the all-surface nature of TMDC MLs makes them extremely sensitive to the surrounding environment and, in particular, to crystal lattice deformations (strain). Strain has, thus, been extensively studied as a tuning knob to gain control over the optoelectronic properties of TMDCs [30], as demonstrated by the considerable variations of the emission energy of excitons in deformed MLs. The strain-induced energy modulation is so large, indeed, that for higher strain values (total strain of about 4%–5%) TMDC MLs undergo a remarkable transition back to an indirect bandgap [39]. The poor radiative efficiency associated to an indirect bandgap is, in principle, not seen favourably; however, for intermediate strain values (around 5%), the PL peaks assigned to indirect excitons feature an intensity reduced by just a factor of about 10 [39]. This relatively modest reduction could be explained by taking into account the effect of the strain-induced hybridisation of direct and indirect excitons in TMDCs [31]. In light of this, strain can be exploited to tune on-demand the recombination energy of TMDCs without remarkable signal losses.

The appearance of lines associated to single-photon emitters (SPEs) in the PL spectra of WSe_2 MLs brought to cryogenic temperatures was reported in 2015 by four different groups [16–19]. The purity of these QEs was assessed via second-order autocorrelation measurements employing Hanbury Brown and Twiss setups [40], with the lines appearing to be spatially localised, spectrally narrow ($\sim$100 μeV), at an energy consistently lower than that of the free-exciton transition, linearly polarised, with lifetimes of 1–10 ns, and featuring Zeeman splittings from which large, very spread-out values of g-factor were extracted. The intimate link between the appearance of these emitters and strain appeared evident from the very beginning, since the SPEs were shown to form preferentially at the flakes' edges [41] or at the border of patterned micrometric holes etched in a silicon substrate [42]. In the following years, emissions from localised excitons were verified also for WS_2 [43, 44], $MoSe_2$ [45–47], MoS_2 [48], for the WSSe alloy [49], and for $MoTe_2$ in the telecom wavelength range [23].

In the case of WSe_2 in particular, the necessity of a strained configuration for the appearance of the emitters has led to a variety of strategies employing etched substrates featuring micro- and nanostructures acting as stressors, on which the TMDC ML is precisely deposited. To name a few, WSe_2 MLs have been deposited on the nanogap between two single-crystalline gold nanorods [50], on top of SiO_2 nanopillars (figures 1(a) and (b)) [33, 51], on platinum nanoparticles—to obtain a high density of emitters [52]—on silver nanoparticles, to generate emitters used in a quantum key distribution experiment to emulate the BB84 protocol using single photons [53], and on several other structures, aiming at enhancing the emission via the Purcell effect (this will be addressed in greater detail in section 4). Strain-localised emitters can also be generated by the surface roughness of glass [54], or by the indentation of an ML, on top of a polymer substrate, via an atomic force microscope (AFM) tip, allowing for the deterministic placement of emitters with nanometric precision [55]. Strain can also be used to gain control over the SPEs' polarisation: bright, linearly polarised emitters can indeed be created by placing a WSe_2 ML on the nanogap of a dielectric rod structure, with the polarisation axis abruptly changing depending on the size of the gap [56]. Another system saw the use of arrays of dielectric square pillars as stressors for a WSe_2 ML, so that at the very edge of the pillar a quasi-1D strain-induced confinement potential was formed, leading to highly linearly polarised (95%) emitters [57].

The origin of these emitters, especially for what concerns the W-based compounds, is still debated, with one of the main hypotheses being the brightening of dark excitons, via the strain-induced hybridisation with defect states [58]. Indeed, due to large spin–orbit coupling, the electronic bands at the K points of the Brillouin zone lift their spin degeneracy, with the valence band experiencing a larger spin splitting than the conduction band [59]. The spins of the so-formed bands alternate with different orders, depending on which of the two unequal K points is being considered [60]. In WSe_2, it has been proved that the bottom conduction sub-band and the top valence sub-band have different spins, making the radiative transition of the actual ground-state spin-forbidden, hence the name dark exciton [61]. The line associated with the bright exciton (that is, the one that is visible in PL) comes from the transition involving the top conduction sub-band and the top valence sub-band, which have the same spin. Tensile strain leads to the lowering of the conduction band, and to a decrease of the bandgap. For certain values of strain (1%–3%) the lower conduction sub-band could reach the energy of a discrete state—caused by a lattice defect—lying inside the bandgap. The hybridisation of the dark exciton with this defect state would relax the selection rules for radiative recombination, leading to the bright emission reported for TMDC SPEs [58]. Although the O-substituted chalcogen vacancy O_{Se} has been proposed as the defect being responsible for this phenomenon [62], the large spread in the values of the g-factor (from -2.02 to -12) extracted from magneto-PL measurements is probably more consistent with the presence of several defect families, all capable of creating QEs [63].

The identification of the point defects responsible for the experimentally reported emissions, together with predictions based on the rational engineering of their properties, is the main effort of *ab initio* computational studies in the field of 2D QEs [64]. For all the practical advantages provided by the low dimensionality of these crystals, equal challenges arise in the computation of their properties, with the

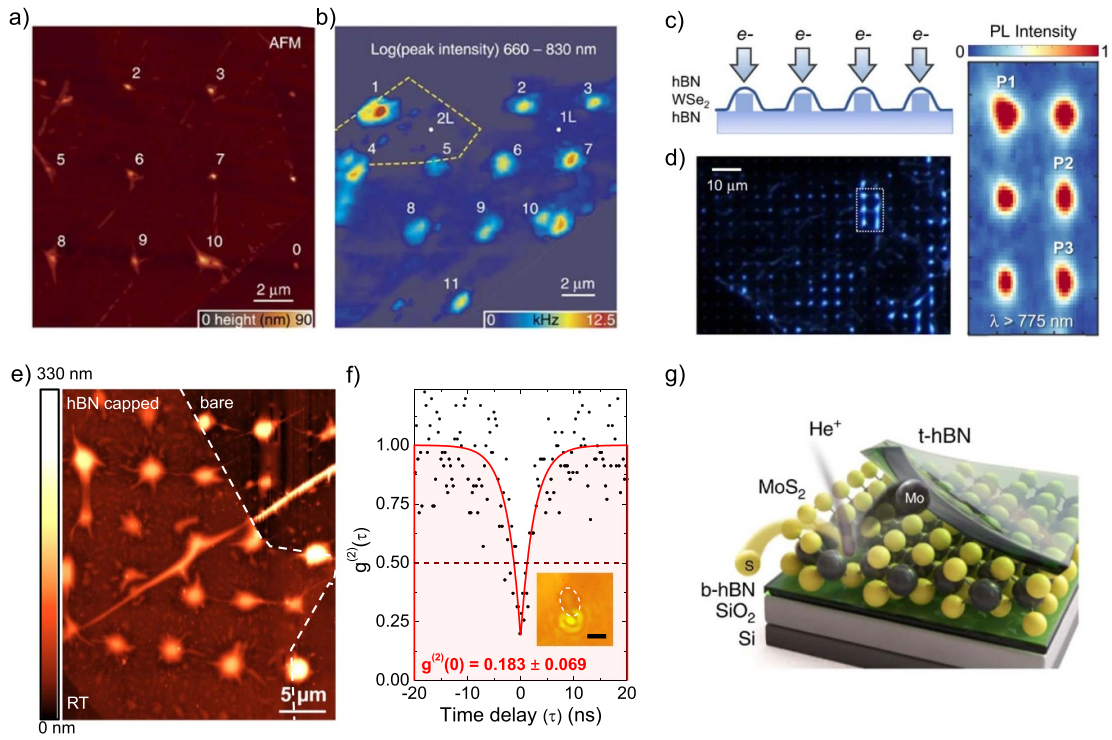

Figure 1. Creation of SPEs in TMDC MLs via strain and defect engineering. (a) AFM image of a WSe_2 ML deposited on top of an ordered array of SiO_2 nanopillars. (b) PL map of the strain-activated QEs, showing the correlation between the bright emission and the nanopillars' location. (a) and (b) Reproduced from [33]. CC BY 4.0. (c) Schematic representation of the creation process of SPEs in WSe_2 via the deposition of an hBN-sandwiched ML on top of an array of dielectric nanopillars, and its subsequent irradiation with an electron beam. (d) PL map showing the appearance of bright emitters at the nanopillars sites, after electron irradiation, demonstrating that the appearance of QEs depends on the presence of both defects and strain in the 2D lattice. On the right, a zoomed-in picture highlights the localised nature of the emission. (c) and (d) Reproduced from [73]. CC BY 4.0. (e) AFM image of an ordered array of hydrogen-filled WS_2 bubbles formed on the surface of a bulk crystal via low-energy proton irradiation. The flake is partially capped with few-layer hBN to prevent the bubbles' deflation at low T. (f) Second order autocorrelation function, showing single-photon emission from a bright narrow line appearing at the edge of a capped WS_2 bubble, as shown in the optical image in the inset. Scale bar, 2 μm. (e) and (f) Adapted from [44]. CC BY 4.0. © 2023 The Authors. Advanced Optical Materials published by Wiley-VCH GmbH. (g) Schematic representation of the formation of QEs in a MoS_2 ML via the creation of chalcogen vacancies with a focused helium ion beam. The ML is then capped with hBN to stabilise the emitters. Reproduced from [48]. CC BY 4.0.

standard density functional theory approach in the mean-field approximation being unable to accurately capture the physical phenomena related to point defects in a 2D host material. To overcome these challenges, associated, in particular, to the anisotropic dielectric screening and strong many-body interactions characterising 2D materials, complex computational approaches are often employed, such as many-body perturbation theory in the GW approximation and the resolution of the Bethe–Salpeter equation for two-particle absorption spectra [64]. To evaluate the formation energy of defects, these are placed in one unit cell at the centre of a larger ensemble of pristine crystal cells, called supercell. In the case of charged defects, the interaction between them and their periodic images leads to large errors, which need to be addressed with a corrective term in the evaluation of the total energy. Such a correction can be obtained by: (i) supercell extrapolation of the analytical expressions relating the supercell size to the electrostatic energies of point charges [65]; (ii) by approximating it to the difference in model charge electrostatic self-energy between isolated and periodic boundary conditions [66–68]; or (iii) by employing self-consistent potential corrections, which prevent the appearance of artificial states in vacuum [69, 70]. For the calculation of the ionisation energy of these defects, it is necessary to take into account electron correlation, which, in the presence of anisotropic screening, requires computationally heavy methods such as GW. To reduce the computational cost of these kinds of evaluations, however, methods based on density functional perturbation theory were successfully employed, in particular for charged defects in hBN [67, 68]. The promising role of *ab initio* calculations for the design of point defects was proven in a work describing in detail the steps necessary for the creation of states meeting the criteria necessary for their use in quantum technologies [71]. In this work, vacancies are identified as good candidates for single-photon emission in several 2D materials. This conclusion is reached through the analysis of the electronic levels of these defects, evaluated with point symmetry group considerations. In particular, the Jahn–Teller distortions caused by the

addition of an electron to the defect are found to originate a two-level system. Ideally, this two-level system needs to be isolated from the band edges of the host crystal, a condition that can be obtained by introducing a paramagnetic impurity next to the vacancy. Gupta *et al* [71] focuses in particular on the $Re_{Mo}V_S$ defect complex in MoS_2, which is found to feature transitions compatible with the optical telecommunication range.

Coming back to the optical activation of the defects, the hypothesis of the hybridisation with a dark state is compatible with the reported difference in energy between WSe_2 strain-localised SPEs and free excitons, since its lower limit of 42 meV is consistent with the splitting between bright and dark excitons [72]. The interplay between strain and defects was also demonstrated in [73], by decoupling these two factors through the fabrication process illustrated in figures 1(c) and (d). Such process involved the deposition of a WSe_2 ML, sandwiched in hBN, on top of silicon nanopillars, followed by its irradiation with an electron beam at 100 keV. The strained, high-quality WSe_2 ML, shielded from substrate effects, showed only a broad defect band prior to irradiation, while the deterministic creation of defects, via the electron beam, led to the appearance of bright lines associated to QEs, which maintained their single-photon nature up to 150 K [73]. Similar results were obtained for a WSe_2 ML deposited on CuO nanoparticles, which showed bright narrow lines in its PL spectrum only after the creation of defects via electron-beam irradiation [74]. All these findings substantiate the hypothesis of a strain-induced brightening of dark excitons, making it the most convincing picture among those proposed in the literature.

Indeed, other hypotheses on the formation of QEs in TMDCs refer to the possibility of creating bound states via sharp strain gradients [75], or, in the case of softer strain profiles over larger areas, to the *funnelling effect* [76], i.e. the drifting of excitons towards points of higher strain (and lower energy gap) and their subsequent trapping by lattice defects. These scenarios, however, need to be reconciled with conflicting experimental results. Indeed, the presence of emitters in nanobubbles formed during the deposition process of WSe_2 MLs due to the trapping of contaminants [77] seems to be in agreement with the identification—via near-field PL measurements performed at RT [78]—of localised, deeply bound excitons at the edge of WSe_2 nanobubbles, and with theoretical calculations suggesting the presence of points of high strain at the nanobubble periphery, due to atomic-scale wrinkling [79]. Moving to the micrometric scale, however, SPEs were also consistently observed on the edges of the hydrogen-filled bubbles that can be formed, in a controlled manner, on the surface of bulk TMDC crystals irradiated with low energy ($\sim$20 eV) hydrogen ions (see figures 1(e) and (f)) [44]. This is partially at odds with the idea that a sharp, nm-scale strain gradient is required for the creation of QEs, given that microbubbles feature a gradual increase of the strain tensor moving from the bubble's edge towards its apex, where the highest strain is reached and where excitons would be expected to funnel [39]. This peculiar spatial dependence of the emission suggests a more complex relationship between the strain values obtained with different methods and the appearance of QEs in W-based compounds.

The origin of the QEs in MoS_2, on the other hand, seems to be mainly connected to the presence of chalcogen-vacancy defects [80], as demonstrated by the deterministic, site-selective creation of emitters via a helium ion beam (a process shown in figure 1(g)) [48], even after encapsulation of the ML in hBN [81, 82]. Vacancy-related defects in MoS_2, $MoSe_2$, WS_2 and WSe_2 can also be created via proton beam irradiation at an energy of 50 keV [83]. Noticeably, proton irradiation can lead to quite opposite effects depending on the beam energy. Low-energy (tens of eV) proton beams were clearly shown not to induce defects in 2D materials [84]; in semiconductor nanostructures, such as self-assembled QDs, proton beams with energies of around a hundred eV were even used to passivate defects and improve their emission efficiency [85]; on the contrary, high-energy (tens of keV) proton-beams can be purposely exploited to create defects acting as QEs in 2D crystal matrices, as shown for different TMDCs [83]. Finally, vacancies in MoS_2 were created also by UV light irradiation [86]. Interestingly, no QEs appear when the UV irradiation takes place in air, since the sulphur vacancies are passivated by oxygen during the formation process, yet the emitters formed in vacuum can be later exposed to air with no repercussions [86]. The site-selective generation of emitters in MoS_2, via a focused helium ion beam, can also be performed after the assembly of a gate-tuneable device for the application of an electric field, showing the emitters' sensitivity to the charge carrier concentration and how they can be turned on and off depending on the applied voltage [87].

The reported emission of the biexciton–exciton cascade in WSe_2 [88] also makes the latter a promising material for quantum technologies based on *photon entanglement*, even though no entangled photon pairs have been reported yet for SPEs based on 2D materials. Photon entanglement is, indeed, at the basis of several areas in the field of quantum technologies, such as quantum metrology and sensing [89–91], quantum communications [92–94] and quantum computing [95, 96]. Unfortunately, the emission lines involved in the cascade are actually doublets characterised by a zero-field fine-structure splitting (FSS) of $\sim$700 μeV [16, 17, 19, 42], which hinders the degree of entanglement of the emitted photons. Since the FSS is thought to be a consequence of the electron–hole exchange interaction in the presence of an anisotropic

potential, the possibility of strain-tuning the emission of these states—using, for example, a piezoelectric substrate [97]—provides us with tools that, in the presence of entangled photons, will enable the reduction of their FSS and the maximisation of their degree of entanglement. A reduction of the FSS by 11% was successfully achieved by employing a device in which the ML was strained by nanopyramid arrays placed on a voltage-controlled cantilever, achieving simultaneous control over the emitters' location, emission energy and splitting [98]. A reduction of the FSS was also obtained through the application of an out-of-plane electric field with a gated device [99]. More in general, electrical manipulation of TMDC SPEs also led to phenomena such as Coulomb blockade, i.e. the loading of single electrons or holes, one by one, into a QE [100]; to the creation of localised trions, featuring a reduced FSS when compared to the neutral exciton species [101]; or to the simultaneous electrical pumping and energy tuning of SPEs via a lateral p–n junction, interfaced with a WSe_2 ML placed on top of a dielectric nanopillar [102]. Moreover, a hybrid electro-optical approach has been recently demonstrated by the appearance of QEs in a WSe_2 ML deposited on a substrate comprised of GaN-based μ-LEDs, operating at low temperatures [103].

Finally, the mechanical manipulation of exfoliated flakes allows for the possibility of stacking layers from different crystals in a predetermined order, easily assembling vertical *heterostructures* (HSs), which host new and interesting phenomena [104]. One of these phenomena is the formation of interlayer excitons (IXs), i.e. excitons in which the electron and the hole are localised in different layers of the HS. IXs are characterised by PL peaks at energies lower than those of the starting materials [105–109], by sublinear power response of their PL intensity, and by longer lifetimes, due to the spatial separation of the two wavefunctions involved in the recombination process [106]. The emission intensity from IXs is heavily dependent on the relative alignment of the two layers' crystal axes (twist angle), with maxima near twist angle values of 0° and 60°, for which the appropriate band alignment in k-space is achieved [110, 111].

The spatial localisation of free IXs can be achieved via strain confinement, as it was the case for a WS_2/WSe_2 heterobilayer deposited on a pillar array [112], by the application of an electric field [113, 114], or by the formation of a *moiré superlattice* potential landscape [115–117]. A moiré potential is the periodic modulation of the electronic band structure due to a lattice mismatch and/or twist angle between the two crystals comprising the HS. This potential is characterised by the presence of points of high symmetry acting as traps for the free IX; the now discrete energy levels can give rise to single-photon emission, as reported for a $MoSe_2/WSe_2$ heterobilayer, with the moiré-trapped QEs featuring circular polarisation, Zeeman splitting upon application of a magnetic field, energy-tuning via the Stark effect, and long lifetimes (∼12 ns) [117].

3. hBN

hBN is a layered crystal whose ML is comprised of a single sheet of alternating boron (B) and nitrogen (N) atoms, arranged in a honeycomb structure akin to that of graphene. Its wide bandgap (∼6 eV) makes it completely transparent in the visible range [118]. Given its chemical inertness and thermal stability [119, 120], hBN is often used as an encapsulating material for other 2D crystals, to improve their electronic and optical properties [121–124]. While the bottom hBN flake provides a smooth surface, free from dangling bonds and charge traps, the top few-layer hBN creates a uniform dielectric environment for the encapsulated crystal [125], protecting the material below from external degradation factors such as oxidation [126] and leading to the narrowing of its PL peaks when compared to an air-exposed sample deposited on a typical SiO_2 substrate [122].

The wide bandgap of hBN is also at the basis of the appearance of colour centres displaying single-photon emission up to RT. While the usage of low-temperature SPEs may still be envisaged for high-end applications—such as quantum cryptography and quantum metrology-requiring the highest brightness and degree of indistinguishability [127], the development of high-quality SPEs working at RT would represent a major breakthrough, allowing for the realisation of scalable, stand-alone photonic circuits with the ability to operate without the aid of external, bulky, and expensive cryogenic systems (either closed-cycle or based on cryogenic liquids). The potential of hBN-based QEs in the field of quantum technologies has been gaining the attention of an increasing number of researchers and is already showing great promise, as confirmed by the use of hBN SPEs for delayed choice experiments [128] and quantum random generation [129], or by the indistinguishability value of 0.56 (corrected by taking into account the non-ideal purity of the single photons), recently measured by Hong–Ou–Mandel interferometry for an hBN SPE [130]. While QEs in W-based TMDCs are likely linked to the presence of dark excitons hybridised with defect states through strain (see previous section), colour centres in hBN are discrete states lying in the middle of the bandgap formed by crystal vacancies or impurities. These 'artificial atoms' embedded in a crystalline matrix are therefore optically active even at RT, with their emission line just broadening due to the increasing phonon population [131]. QEs in hBN have been found in its ML form [20], as well as in bulk crystals [21, 22], with their zero-phonon line (ZPL) spanning the whole visible spectrum [131, 132] (as can

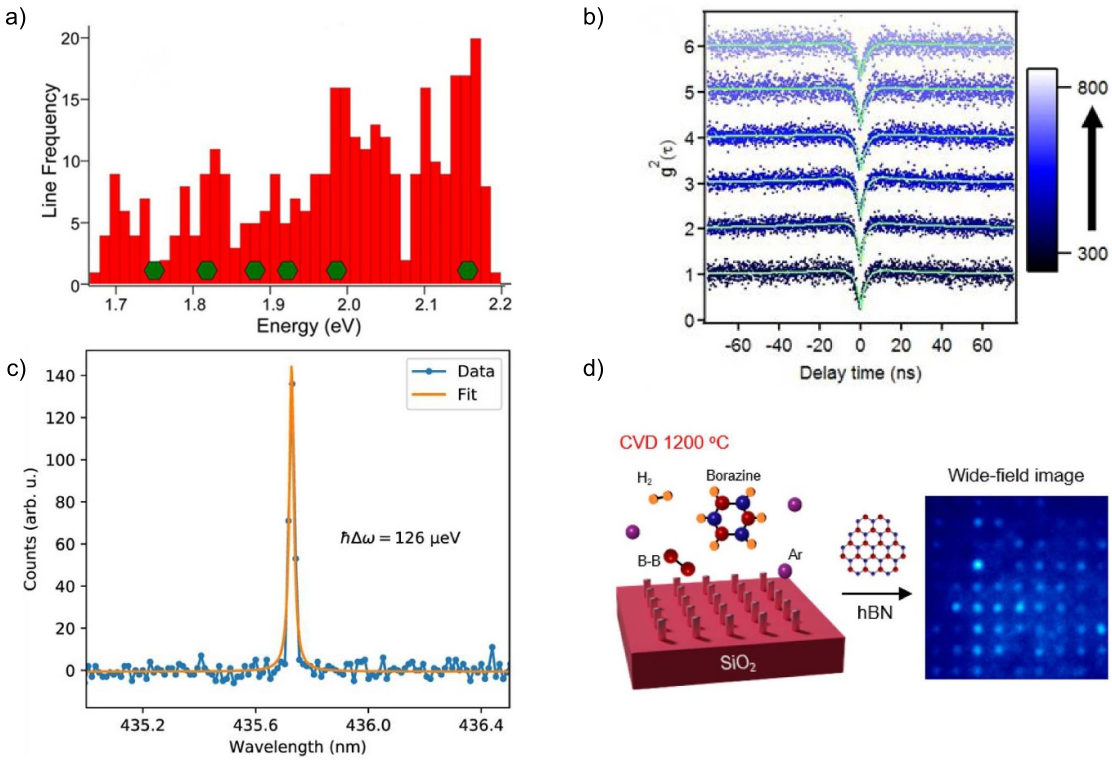

Figure 2. Quantum emitters in hBN. (a) Histogram of the QE energy of 90 different multilayer hBN flakes, spanning a wide energy range. The green hexagons indicate the lines for which single-photon emission has been verified via autocorrelation measurements. Reprinted with permission from [131]. Copyright (2016) American Chemical Society. (b) Second-order autocorrelation function $g^2(\tau)$, showing robust single-photon emission from a line in the spectrum of an hBN flake, measured from 300 K to 800 K with steps of 100 K. Reprinted with permission from [134]. Copyright (2017) American Chemical Society. (c) Low temperature, resolution-limited PL line from a colour centre created with submicrometric precision via the electron beam of a scanning electron microscope. Reproduced from [143]. CC BY 4.0. (d) Schematic representation of the direct CVD-growth of hBN flakes on top of SiO_2 nanopillars and wide-field PL image showing the strain-activated quantum emitters. Reprinted with permission from [151]. Copyright (2021) American Chemical Society.

be seen in the histogram of figure 2(a)) up to the UV region [133], and still maintaining single-photon purity up to 800 K [134], as confirmed by the second-order autocorrelation measurements reported in figure 2(b). Even though emitters can also be found in as-grown crystals [21, 135], several strategies have been employed to increase their density and/or efficiency in a controlled manner.

Annealing at high temperatures in argon has been found to be the most reliable procedure to optically activate QEs in hBN [20, 22], be they naturally occurring or induced. Emitters related to lattice defects can be successfully obtained by chemical etching [136], ion irradiation [137–139], electron beam irradiation [132, 138], laser ablation [138], plasma treatment [140–142], even reaching submicrometre precision in the positioning of the colour centres by employing the electron beam of a scanning electron microscope [143] (figure 2(c)). High energy (MeV) electron irradiation has been shown to lead to the formation of stable SPEs, with no need for annealing in Ar atmosphere, in a variety of exfoliated multilayers (high purity, B enriched, C enriched) as well as chemical vapour deposition (CVD)-grown MLs [144]. On the other hand, laser irradiation appears to yield better results in multilayer flakes, with purer emitters displaying brighter and sharper lines when compared to those observed in large MLs, which are affected by a hexagonal-to-cubic lattice structure transition [145]. The effects of different types of irradiations can be unveiled by monitoring the emission from the colour centres on samples undergoing layer-by-layer etching with O_2 plasma: by keeping track of the number of layers that need to be etched away before the disappearance of the emitter, it has been found that the centres created by other plasma treatments tend to form on the crystal surface, while electron irradiation leads to emitters located throughout the whole crystal [146]. By performing large area PL maps, the different roles played by low-energy electron irradiation and annealing were clearly identified, with the former being responsible for the creation of new emitters and the latter for the brightening of those already present [147].

Strain can be used as a tuning knob for the emission—as it is the case for flakes on bendable polycarbonate beams, where the emitters were formed by He ion irradiation [148]—but it also seems to play a role in the creation of the defects themselves, as demonstrated by the similar spectral features of QEs in

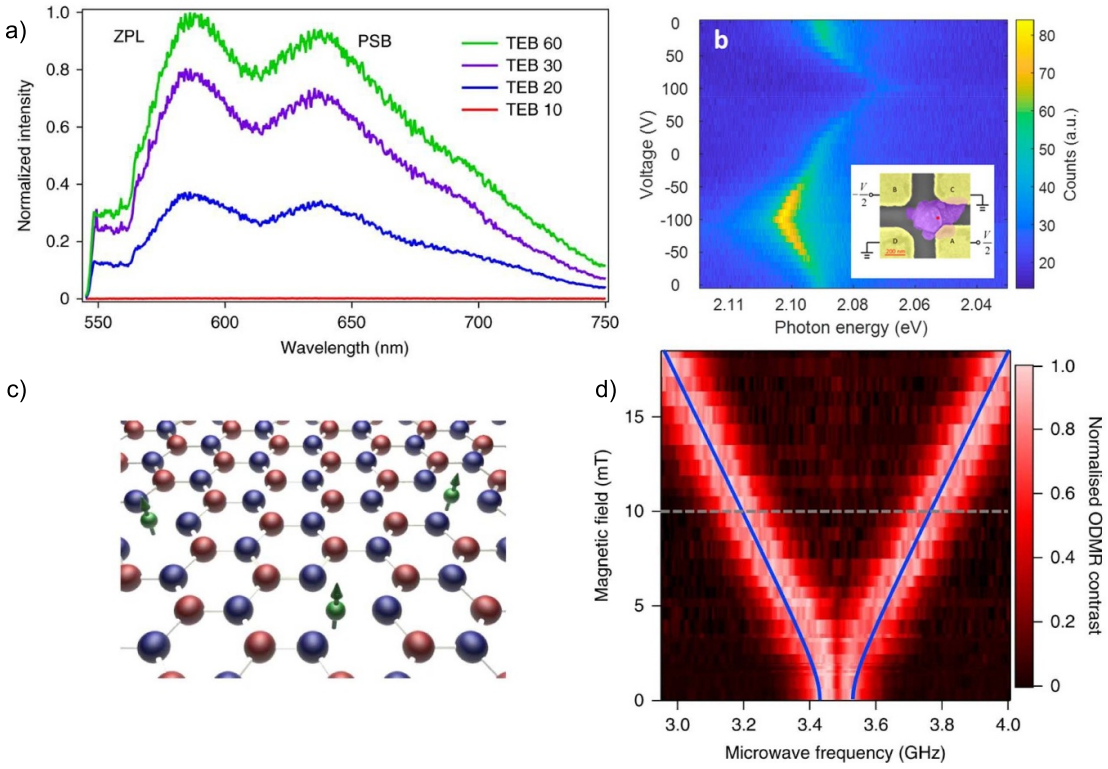

Figure 3. Control over the emission properties of hBN QEs and spin defects. (a) PL spectra showing carbon-related defects' ZPLs and their phonon side bands (PSBs) for increasing concentrations of carbon during the growth process. Reproduced from [157], with permission from Springer Nature. (b) Stark shift of an emitter's ZPL as a function of the voltages applied to electrodes A and B of the device shown in the inset. The Stark shift of up to 31 meV is four-fold the FWHM of the ZPL at RT. Reprinted with permission from [170]. Copyright (2019) American Chemical Society. (c) Lattice representation of the spin defect V_B^-. Boron (nitrogen) atoms are represented by red (blue) spheres. (d) ODMR contrast shift of the V_B^- defect for increasing magnetic field. (c) and (d) Reproduced from [190], with permission from Springer Nature.

untreated BN nanotubes and hBN flakes deposited on diamond nanopillars [149], by the activation yield of 10% of single QEs in flakes deposited on silica nanopillars [150] jumping to 80% when flakes are CVD-grown directly on pillars of 250 nm of diameter [151] (schematic representation in figure 2(d)), or by the appearance of emitters by nanoindentation with an AFM tip [152]. A 31% yield of single QEs was also achieved by the deterministically controlled creation of edges via the patterned milling of hBN using a gallium focused beam [153]. The link between strained configurations, such as those arising from the wrinkling of the material, and the polarisation axis of the emitters appears evident in samples brought to low temperature (10 K) in which the QEs' polarisation aligns with the wrinkle direction [154].

Given the very broad range of emission of QEs in hBN, several different strategies to gain control over their properties have been developed. An optimised CVD growth technique leads to the formation of multilayer hBN displaying the majority of the emitters at a wavelength of the ZPL of 580 ± 10 nm, greatly reducing the emitters' variability in energy and suggesting that this particular wavelength range is associated to a specific crystal defect related to the growth process [155]. Even CVD-grown MLs, featuring large homogeneous domains, display emitters at a wavelength of 575 ± 15 nm, with no need for ion irradiation or annealing in argon [156]. The presence of carbon during other growth techniques (metallorganic vapour phase epitaxy and molecular beam epitaxy) appears to be crucial for the appearance of SPEs (as shown in figure 3(a)), with the $V_BC_N^-$ defect as a possible candidate [157], confirming several theoretical studies on the role of carbon [158–167], which also attributed the UV emission at 4.1 eV to the carbon dimer defect C_BC_N [168]. Control over the emitters wavelength has been partially achieved (*i*) via the Stark effect, tuning the emission with an out-of-plane electric field applied by graphene gates [169]; (*ii*) with a four-electrode device controlling both the amplitude and the direction of the electric field, leading to a Stark shift (visible in figure 3(b)) four times larger than the full width at half maximum (FWHM) at RT [170]; or (*iii*) by placing the emitters between an indium tin oxide coated glass slide and a conductive AFM tip [171]. Substrate engineering has also been explored as a possible approach to gain control over the emitters' properties. Even though emitters in suspended thin films, which do not suffer from any substrate-induced effect, still show a large variability in their spectral, temporal and spatial characteristics [172], surface passivation of a SiO_2

substrate with Al_2O_3 leads to the appearance of QEs with ultranarrow ZPLs (45 μeV), almost no sidebands and a g-factor of just 0.2, making them nonmagnetic [173]. A shift of the ZPL wavelength from 600–650 nm to 550–600 nm takes place when nickel is used, instead of quartz, as a supporting substrate for multilayer hBN grown by CVD on copper [174]. Controlled localisation of the emitters, on the other hand, is achieved by patterning openings in a graphene layer put on top of three-layer hBN [175]. This exploits the graphene-induced suppression of emitters, which takes place via a double transfer mechanism: an energy transfer is responsible for the intensity reduction of all ZPLs, while a charge transfer is responsible for the complete quenching of all the ZPLs beyond 600 nm [176].

The substrate on which hBN flakes are deposited appears to be important also for what concerns the broadening of the emitters' linewidth. Even at cryogenic temperatures, linewidths of 27 μeV have been interpreted as a consequence of ultrafast spectral diffusion [177], i.e. the variation of the electric field around the emitters, leading to small changes in the emission wavelength and, thus, the broadening of the peak. This phenomenon, in the case of hBN, is thought to be linked to two dephasing mechanisms, which according to [178] occur at two different timescales ($\sim$20 μs and $\sim$500 μs). Similar linewidths were also reported in the case of resonant excitation [179], while reduced linewidths were obtained by performing photoluminescence excitation (PLE) measurements on resonance with the ZPL, while monitoring the intensity of the phonon sideband, at low power excitation [180], by using conductive indium tin oxide as a substrate instead of SiO_2 [181] or by low-power resonant excitation [182]. The goal of Fourier transform (FT)-limited linewidths of $\sim$0.21 μeV was initially achieved at low temperatures by resonant excitation of flakes deposited on a silver mirror and annealed further to eliminate chemical residues [183], or by two-laser resonant repumping [184]. FT-limited lines were reported also at RT, suggesting the presence of spectral diffusion but the complete lack of phonon dephasing [185, 186]. This was interpreted as the consequence of the decoupling of the defect with low-frequency in-plane acoustic phonons, due to an out-of-plane lattice distortion [185, 186].

Even though QEs in hBN generally show non-magnetic behaviour [187], the magnetic field-dependent variation of the steady-state, RT PL observed for a small fraction of QEs has been interpreted as a consequence of the presence of optically addressable spin defects [188]. This kind of defects could play a major role not only in the field of quantum sensing, given their extreme sensitivity to local magnetic fields and temperature, but also in quantum computing and communication, exploiting the optical initialisation and readout of spin quantum memory [189]. An ensemble measurement performed at RT on a PL line attributed to the V_B^- defect (whose lattice structure is shown in figure 3(c)) featured a triplet groundstate with a zero-field splitting of 14 μeV and optically detected magnetic resonance (ODMR) (whose dependence on the applied magnetic field is reported in figure 3(d)) [190]. Going to low temperatures the V_B^- excited state also showed ODMR, with the state being confirmed as a triplet featuring a longitudinal splitting of 8.93 μeV and a g-factor of 2 [191]. The photodarkening of the emitters at 3.5 K, going from an out-of-plane magnetic field of 0 T to 7 T is consistent with a picture in which the spin-dependent non-radiative intersystem crossing transitions happen from the triplet excited state to the lowest-lying spin-singlet metastable, and then from the metastable state to the triplet ground state [192]. Carbon-related defect ensembles feature ODMR at RT as well [157, 193], which is correlated to a second bunching timescale in the second-order autocorrelation function $g^2(\tau)$ [193], while a still unidentified paramagnetic defect, which is known to be neither V_B^- nor carbon related, also features ODMR and has a g-factor of 2 [137].

4. Integration with plasmonic and photonic structures

Being embedded in a 2D matrix, QEs in TMDCs and hBN are particularly well-suited for the integration in photonic and plasmonic cavities, to which they can be deterministically coupled via simple dry transfer methods. These cavities aim at improving the emitters' performances in terms of brightness and photon collection via the Purcell effect [194]. The Purcell effect is the modification of an emitter's radiative rate by controlling its environment, with the two major strategies employed by research groups being the use of plasmonic cavities, which exploit the interaction with plasmons forming at the surface of metallic nanostructures, and photonic cavities, in which the electromagnetic field is confined and amplified. Since 2D crystals lack internal reflection, they can be efficiently interfaced with these cavities by simply depositing the ML on top of the desired structure; moreover, taking into consideration the need for a strained configuration for the activation of the QEs (as far as W-based TMDCs are concerned), it is only natural that the plasmonic/photonic structures, designed for the enhancement of the radiative recombination rate of the emitters, serve also the purpose of acting as stressors for the deposited MLs. As far as hBN is concerned, one basic difference between this system and TMDCs gives rise to an ulterior advantage in using hBN QEs: while emitters in TMDCs are of excitonic nature and are localised by strain-induced potential minima and/or crystal defects, SPEs in hBN are colour centres for which discrete states, caused by crystal defects, lie in the middle of hBN's wide bandgap of 6 eV. This fact decouples almost completely the properties of the QEs

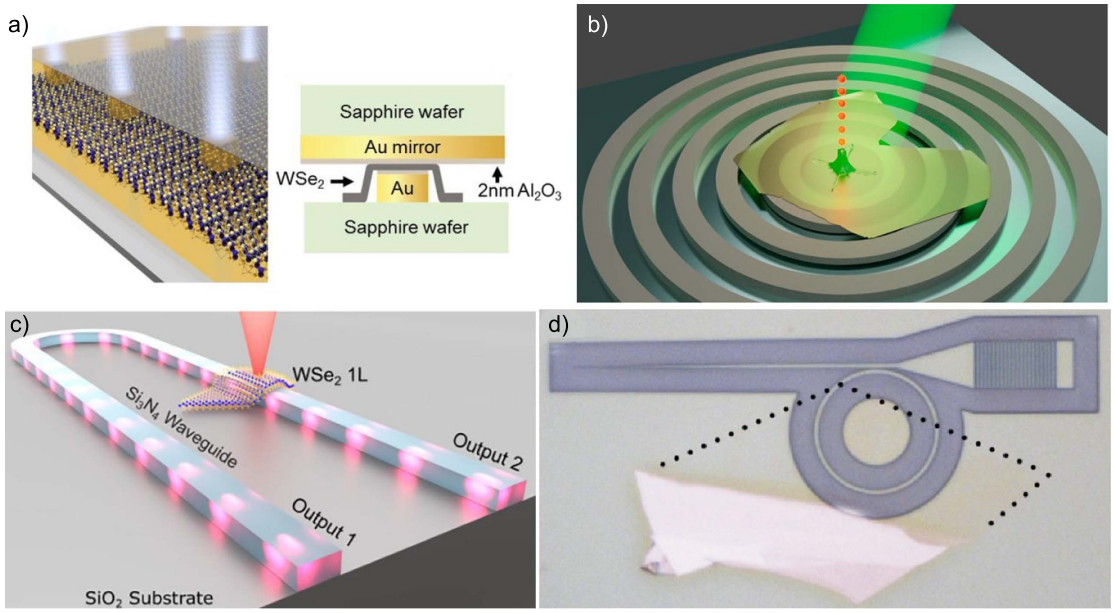

Figure 4. Integration of TMDC QEs in cavities for the enhancement of their radiative emission. (a) Plasmonic structure comprised of a WSe_2 ML placed in the nanogap between a gold nanocube, acting also as a stressor, and a gold mirror. Reproduced from [200]. © IOP Publishing Ltd. All rights reserved. (b) WSe_2 ML placed on top of a dielectric nanopillar at the centre of a circular Bragg grating (bullseye) cavity. Reprinted with permission from [202]. Copyright (2021) American Chemical Society. (c) WSe_2 ML deposited on top of a silicon nitride waveguide. The waveguide's output can also be employed to resonantly excite the emitters. Reproduced from [210]. CC BY 4.0. (d) Optical image of a WSe_2 ML coupled to a microring resonator. The σ^+ polarised emission from the QEs couples to the mode of the outer ring. Reprinted with permission from [211] © The Optical Society of America.

found in hBN from the evolution of the electronic bands of the host, which, conversely, plays a major role in TMDCs: in TMDCs, indeed, SPEs can be found almost exclusively in MLs, which are characterised by a direct bandgap in the K points of the Brillouin zone. For this reason, TMDC-based plasmonic and photonic cavities necessarily involve a TMDC ML interfaced with bulk elements made from other materials, i.e. a hybrid platform. hBN, on the other hand, is not constrained by limitations on the flake thickness, with bright emitters forming even in bulk crystals. Even though a thin crystal leads to a reduced total internal reflection and, thus, an increased extraction efficiency, one can deal with hBN flakes that are just thick enough for the creation of monolithic cavities, *i.e.* a platform in which both the emitters' host and the cavity elements are made with the same crystal, thus removing the photonic losses at the interfaces between different materials.

4.1. TMDCs

A plasmonic coupling-induced reduction of the lifetime of the emitters, leading to an enhanced brightness, was observed for WSe_2 MLs deposited on silver nanowires [195], silver-Al_2/O_3 nanocones [196], gold nanorods [197], Al_2O_3/Au nanopillars [198], gold nanocubes coupled to gold mirrors, shown in figure 4(a), [199] (a type of cavity which can maintain single-photon emission up to 160 K, given the right growth conditions for the ML [200]) and gold nanostars [201]. Despite their small mode volumes, plasmonic cavities are affected by losses that reduce their Purcell factor, i.e. the number quantifying the emission rate enhancement. To limit these losses, dielectric materials have also been explored as candidates for the creation of cavities. The desired enhancement was achieved for a WSe_2 ML deposited on top of a dielectric nanopillar at the centre of a circular Bragg grating ('bullseye') cavity (figure 4(b)), obtaining lifetime reductions of one order of magnitude [202]. An increased quantum efficiency was also achieved for GaP nanoantennas [203], while silicon nitride dimer nanoantennas, with square cross-section, not only led to a reduction of the SPEs' lifetimes, but also provided control over the emitter polarisation by varying the dimer orientation [204]. Optical cavities employing distributed Bragg reflectors also led to emission enhancements [205], which become even more drastic when an adjustable top mirror allows for the precise tuning of the Fabry–Perot cavity [206].

The creation of on-chip photonic integrated circuits would greatly improve the production, scalability, and compactness of devices exploiting QEs in TMDCs for quantum technologies, via the miniaturisation of optical quantum circuits. To this end, TMDC QEs need to couple to photonic waveguides, as it was demonstrated for gold [207], SiN [208] and Ti in-diffused lithium niobate waveguides [209]. The waveguides not only provide the geometry to strain the MLs that are deposited on top of them, but, as shown

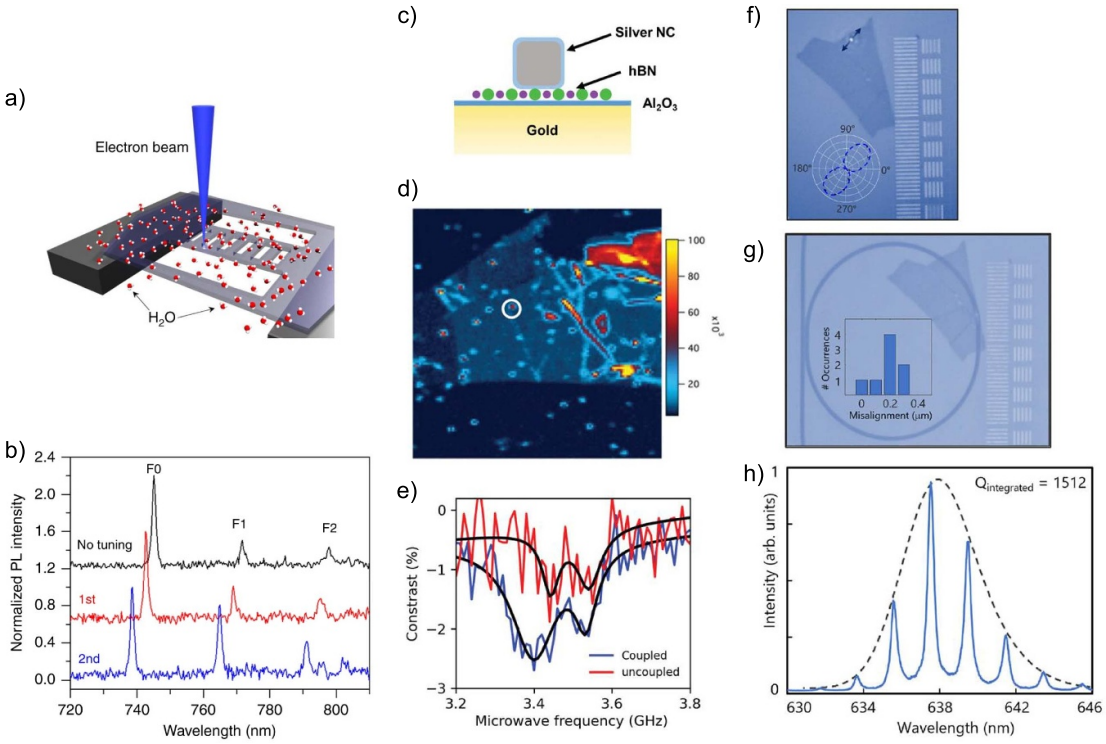

Figure 5. Integration of hBN QEs with plasmonic and photonic cavities. (a) Monolithic 1D photonic cavity of the ladder type. The cavity resonance can be tuned by scanning a focused electron beam along the outer walls of the nanocavity in the presence of water molecules, in order to activate the etch reaction. (b) PL spectra of emitters before (black) the tuning process and after the first (red) and second (blue) tuning steps. (a) and (b) Reproduced from [212]. CC BY 4.0. (c) Schematic representation of a plasmonic cavity comprised of an hBN flake deposited on a Al_2O_3 film on top of a gold surface, and topped by a silver nanocube. (d) PL intensity map of an hBN flake in the plasmonic cavity. The white circle indicates an area in which the V_B^- spin defect coupled to the plasmonic resonance. (e) ODMR spectrum of a V_B^- spin defect uncoupled (red) and coupled (blue) to the cavity, showing an enhancement of the contrast. (c)–(e) [218] John Wiley & Sons. © 2021 Wiley-VCH GmbH. (f) Characterisation of the polarisation axis of an emitter in an hBN flake near positioning markers. (g) Optical image of a completed device in which the emitter is integrated and dipole-aligned with the microring resonator cavity. The inset shows the number of occurrences for different values of misalignment between the QEs and the resonators. (h) Characterisation of a microring resonator. A broadband diode (dashed line) is coupled to the output port of the waveguide, while the scattered light from the ring (solid line) is collected with an objective. A *Q*-factor of 1512 is measured. (f)–(h) Reproduced from [222]. CC BY 4.0.

for the horseshoe device in figure 4(c), they can also be used to resonantly excite the emitters by shining the laser on one of the waveguide's outputs; while the laser light remains confined in the waveguide, the single photons from the ML are collected with an optical objective on top of the crystal [210]. Finally, microring resonators can couple to the chiral emission of TMDC MLs [211]. Indeed, the two unequal K points of the Brillouin zone are characterised by emissions of light that is either right-circularly polarised or left-circularly polarised. In the presence of a magnetic field, these two polarisations experience a Zeeman splitting in energy, the QE's σ^+ peak can then couple to the σ^+ mode of the outer ring of the resonator, while the scatterers in the inner ring emit spin converted σ^- light (figure 4(d) [211].

4.2. hBN

An hBN monolithic photonic crystal cavity featuring a high quality (*Q*-)factor, consisting of a 1D structure (ladder type), was formed via reactive ion etching and electron beam induced etching (EBIE). Reducing the cavity width via EBIE allowed for the tuning of the 1D modes after the identification and characterisation of the emitters [212] (figures 5(a) and (b)). An hBN monolithic bullseye cavity, on the other hand, not only showed an enhancement of the PL signal, but also better contrast in the ODMR measurements of spin defects [213], while a Purcell factor of 15 was achieved for a monolithic crystal cavity for which the coupling with the SPEs was tuned via gas condensation [214].

For what concerns the Purcell effect caused by plasmonic enhancement of the emitters intensity in hBN crystals, this was reported for flakes wet-transferred on periodic gold and silver nanoparticle arrays [215], for emitters near gold nanospheres which were precisely positioned via an AFM tip [216] and for silver nanopillars, which also acted as stressors [217]. Plasmonic effects on the enhancement of the ODMR contrast of V_B^- defects were also reported for silver nanocubes [218] (figures 5(c)–(e)) and for gold film microwave waveguides [219]. The precise ZPL wavelength of this spin defect, which is otherwise

characterised by a broad emission, could be determined by tuning the coupling with a high-Q nanobeam cavity, while monitoring the resonance intensity, yielding a value of 773 ± 2 nm [139].

Single photons from hBN have been coupled to AlN waveguides (as demonstrated by the spatial separation between the points of excitation and collection) showing, however, a 1.35% efficiency, when compared to a confocal configuration [220]. A monolithic approach can also be applied to waveguides, with the QEs placed in the middle of the structure and the collection taking place from the two side grating couplers [221]. A striking 46% coupling efficiency was obtained with a waveguide coupled to a microring resonator made from Si_3N_4, with the coupling being deterministic, since the silicon nitride structure is grown after the identification of the emitter's position and of its dipole alignment [222] (a process that is shown in figures 5(f)–(h)).

Other optical cavities, which have been used to increase the radiative efficiency of QEs in hBN, and which are worth mentioning, include plane concave microcavities (leading also to narrower and purer SPEs) [223], CVD-grown hBN multilayer transferred to Si_3N_4, where the cavity is then designed with electron-beam lithography (EBL) [224], strain-activated emitters from hBN wrapped around Si_3N_4 microdisc optical resonators [225] and few-layer CVD-grown hBN coupled to a hybrid open fibre-coupled Fabry–Perot cavity, allowing for strong linewidth reduction, broad spectral tuning range from 565 nm to 635 nm and enhancement of the ZPL up to 50 fold [226].

5. Conclusions

Since their discovery, less than a decade ago, QEs in 2D materials (2D QEs) have endured a tumultuous development, retracing, if only at an accelerated pace, much of the trail blazed by III–V QDs in the preceding 20 years. As a direct consequence of this research effort, the peculiarities and differences between QEs hosted by TMDCs and hBN have been thoroughly explored and exploited accordingly. To summarise, TMDC QEs, especially in the case of W-based compounds, are thought to be the result of a strain-induced hybridisation of dark excitons and defect states [58], and as such they emerge mainly in the ML form of these crystals, characterised by efficient light emission [34, 35]. On the other hand, hBN QEs are colour centres, i.e. defect states lying deep in the middle of the large bandgap of the host crystal [118]. As a result, not only hBN does not need to be in the ML form to feature QEs, but these QEs are robust to thermal fluctuations, with single-photon emission maintaining its purity even at RT. On the other hand, TMDC QEs appear mainly at cryogenic temperatures, with only hBN-sandwiched high quality WSe_2 samples featuring SPEs up to 150 K [73]. QEs hosted by TMDCs emit, for the most part, in the visible range (620–780 nm), with the notable exception of $MoTe_2$, which features emitters in the telecom range 1080–1550 nm [23]; hBN QEs, on the other hand, span the whole spectrum from UV to NIR. A plethora of methods have been employed to create defects in the crystalline structure of these materials, while their activation relies on annealing at high temperatures, in the case of hBN [20], and on the creation of strained configurations for W-based TMDCs, whether by deposition on etched substrates acting as stressors [33], by indentation with AFM tips [55], or by pressure-induced bulging of the crystal surface [44]. The strategies for the creation/activation of the emitters, as well as their main properties, have been the object of extensive discussions in sections 2 and 3. Even though—as discussed above—some work remains to be done in order to match the performances of these quantum sources to those of the state-of-the-art single-photon sources based on InGaAs *et similia*, 2D QEs are already at a point where some of the inherent advantages of this material platform can be exploited to push forward the field of quantum technologies as a whole. From a sustainability point of view, for example, TMDCs and hBN crystals are comprised of chemical elements which are relatively available, with MoS_2 being found in nature in the form of the molybdenite mineral. These features are in stark contrast with the availability of gallium and indium and, more in general, with the poor sustainability of the production process of QDs based on III–V materials. As yet another sign of the potential of 2D QEs, it is worth stressing here, for one last time, that the recent discovery of optically addressable spin defects in hBN [190] carries great importance, due to its promise for the realisation of spin-photon interfaces and for quantum sensing. Moreover, as noted in the previous section, the ease with which 2D crystals can be mechanically transferred onto the substrate of choice entails the possibility to deterministically integrate 2D QEs with all kinds of photonic and electronic devices. The potential advantages of the coupling with photonic structures have been thoroughly discussed in section 4, and basically boil down to the possibility of enhancing and optimising the performances of 2D QEs via the Purcell effect—for photonic microcavities—and to the realisation of integrated photonic circuits, for the on-chip implementation of quantum computation protocols. As far as electronic devices are concerned, on the other hand, we would like to briefly note the intriguing possibilities opened by the recent coupling of TMDC-based QEs with GaN micro-LEDs, as detailed in [103]. If paired with one of the several methods developed to control the position of 2D QEs, this result could lead to the fabrication of ordered arrays of individually addressable, electrically pumped single-photon sources. Indeed,

this system would present several advantages if compared to QDs, such as the fact that QEs in 2D materials are not affected by thermalisation between different emitters, which is instead typical of self-assembled QD ensembles [227]. Of course, in order to truly help the development of the complex photonic circuits required for the advancement of quantum technology, the fabricated QE arrays should all emit identical photons. Considering the large spreads almost universally characterising the emission energy of 2D QEs (see, e.g. figure 2(a)), the fulfilment of this strict requirement will likely demand the development of effective post-fabrication methods to control, first of all, the energy of individual QEs, but also their other degrees of freedom, such as polarisation and spatial mode. As noted in the previous sections, strain engineering is one of the most promising tools for the fine-tuning of the emission properties of 2D QEs. The most advanced strain-engineering protocols are currently based on the emitter's integration with micro-machined piezoelectric actuators, whose simultaneous integration with 2D QEs, micro-LEDs, and/or complex photonic circuits poses severe technological challenges, which may well prove too hard to overcome; in this case, the issue may be circumvented by resorting to other methods to tune the emitters, e.g. Stark tuning, which only requires encapsulating the QE-containing 2D layer between graphene electrodes [169].

In summary, one could say that the defining trait of QEs embedded in 2D crystals—as, we hope, is clearly evidenced by many of the examples provided in the previous paragraphs—is represented by their *flexibility*, to be intended not only literally, but also in the sense of their extreme adaptability. This feature, which makes it comparatively simple to find creative solutions to any of the issues limiting the performance of devices based on 2D QEs, will represent an invaluable tool in our journey towards the realisation of optimised single-photon sources, as required by future quantum-technology applications.

Data availability statement

No new data were created or analysed in this study.

Acknowledgments

The authors would like to acknowledge helpful discussions with Antonio Polimeni and Giorgio Pettinari. S C and E B acknowledge support from La Sapienza through the grants Avvio alla Ricerca 2022 (Grant No. AR122181681D6C44) and Avvio alla Ricerca 2021 (Grant No. AR12117A8A090764), respectively. E B has also received funding from the Nano Letters Seed Grant 2022 by the American Chemical Society. M F acknowledges financial support from the PNRR MUR Project PE0000023-NQSTI, from Sapienza Progetti H2020-Collaborativi (No. PH120172B8A67DD1), from Sapienza Progetti di Ricerca 2021 (No. RP12117A8B4C9CA8), and from Sapienza Progetti di Ricerca 2022 (No. RM1221816B7BAEFD). This project was also funded within the QuantERA II Programme that has received funding from the European Union's Horizon 2020 research and innovation programme under Grant Agreement No. 101017733, and with funding organisations Ministero dell'Università e della Ricerca and Consiglio Nazionale delle Ricerche.

ORCID iDs

Salvatore Cianci https://orcid.org/0000-0003-4020-369X
Elena Blundo https://orcid.org/0000-0003-0423-4798
Marco Felici https://orcid.org/0000-0002-0977-2301

References

[1] Aharonovich I, Englund D and Toth M 2016 Solid-state single-photon emitters *Nat. Photon.* **10** 631–41
[2] Senellart P, Solomon G and White A 2017 High-performance semiconductor quantum-dot single-photon sources *Nat. Nanotechnol.* **12** 1026–39
[3] Gurioli M, Wang Z, Rastelli A, Kuroda T and Sanguinetti S 2019 Droplet epitaxy of semiconductor nanostructures for quantum photonic devices *Nat. Mater.* **74** 1–12
[4] Surrente A, Felici M, Gallo P, Rudra A, Dwir B and Kapon E 2017 Dense arrays of site-controlled quantum dots with tailored emission wavelength: growth mechanisms and optical properties *Appl. Phys. Lett.* **111** 221102
[5] Felici M *et al* 2020 Broadband enhancement of light-matter interaction in photonic crystal cavities integrating site-controlled quantum dots *Phys. Rev.* B **101** 205403
[6] Biccari F *et al* 2018 Site-controlled single-photon emitters fabricated by near-field illumination *Adv. Mater.* **30** 1705450
[7] Liu J *et al* 2019 A solid-state source of strongly entangled photon pairs with high brightness and indistinguishability *Nat. Nanotechnol.* **14** 586–93
[8] Hennessy K, Badolato A, Winger M, Gerace D, Atatüre S G M, Fält S, Hu E L and Imamoğlu A 2007 Quantum nature of a strongly coupled single quantum dot-cavity system *Nature* **445** 896–9
[9] Somaschi N *et al* 2016 Near-optimal single-photon sources in the solid state *Nat. Photon.* **10** 340–5
[10] Uppu R *et al* 2020 Scalable integrated single-photon source *Sci. Adv.* **6** eabc8268

[11] Frenzel M, Mikolajczak C, Reuter M A and Gutzmer J 2017 Quantifying the relative availability of high-tech by-product metals—the cases of gallium, germanium and indium *Resour. Policy* **52** 327–35
[12] Blundo E, Yildirim T, Pettinari G and Polimeni A 2021 Experimental adhesion energy in van der Waals crystals and heterostructures from atomically thin bubbles *Phys. Rev. Lett.* **127** 046101
[13] Novoselov K S, Geim A K, Morozov S V, Jiang D-en, Zhang Y, Dubonos S V, Grigorieva I V and Firsov A A 2004 Electric field effect in atomically thin carbon films *Science* **306** 666–9
[14] Bandurin D A *et al* 2017 High electron mobility, quantum Hall effect and anomalous optical response in atomically thin InSe *Nat. Nanotechnol.* **12** 223–7
[15] Leng K, Wei F, Liu Y, Chhowalla M and Ping Loh K 2020 From bulk to molecularly thin hybrid perovskites *Nat. Rev. Mater.* **5** 482–500
[16] Srivastava A, Sidler M, Allain A V, Lembke D S, Kis A and Imamoğlu A 2015 Optically active quantum dots in monolayer WSe_2 *Nat. Nanotechnol.* **10** 491–6
[17] Yu-Ming H *et al* 2015 Single quantum emitters in monolayer semiconductors *Nat. Nanotechnol.* **10** 497–502
[18] Maciej Koperski K N, Ashish Arora V C, Paul Mallet J-Y V, Marcus J, Kossacki P and Potemski M 2015 Single photon emitters in exfoliated WSe_2 structures *Nat. Nanotechnol.* **10** 503–6
[19] Chakraborty C, Kinnischtzke L, Goodfellow K M, Beams R and Nick Vamivakas A 2015 Voltage-controlled quantum light from an atomically thin semiconductor *Nat. Nanotechnol.* **10** 507–11
[20] Tran T T T, Bray K, Ford M J, Toth M and Aharonovich I 2016 Quantum emission from hexagonal boron nitride monolayers *Nat. Nanotechnol.* **11** 37–41
[21] Javier Martínez L, Pelini V W T, Maze J R, Gil B, Cassabois G and Jacques V 2016 Efficient single photon emission from a high-purity hexagonal boron nitride crystal *Phys. Rev.* B **94** 121405
[22] Tran T T T, Zachreson C, Michael Berhane A M, Bray K, Sandstrom R G G, Li L H, Taniguchi T, Watanabe K, Aharonovich I and Toth M 2016 Quantum emission from defects in single-crystalline hexagonal boron nitride *Phys. Rev. Appl.* **5** 034005
[23] Zhao H, Pettes M T, Zheng Y and Htoon H 2021 Site-controlled telecom-wavelength single-photon emitters in atomically-thin $MoTe_2$ *Nat. Commun.* **12** 6753
[24] Silverstone J W, Bonneau D, OBrien J L and Thompson M G 2016 Silicon quantum photonics *IEEE J. Sel. Top. Quantum Electron.* **22** 390–402
[25] Felici M, Birindelli S, Trotta R, Francardi M, Gerardino A, Notargiacomo A, Rubini S, Martelli F, Capizzi M and Polimeni A 2014 Nanoscale tailoring of the polarization properties of dilute-nitride semiconductors via H-assisted strain engineering *Phys. Rev. Appl.* **2** 064007
[26] Castellanos-Gomez A, Roldán R, Cappelluti E, Buscema M, Guinea F, Herre S J van der Z and Steele G A 2013 Local strain engineering in atomically thin MoS_2 *Nano Lett.* **13** 5361–6
[27] Desai S B, Seol G, Seuk Kang J S, Fang H, Battaglia C, Kapadia R, Ager J W, Guo J and Javey A 2014 Strain-induced indirect to direct bandgap transition in multilayer WSe_2 *Nano Lett.* **14** 4592–7
[28] Ryu Y K K, Carrascoso F, López-Nebreda R, Agraït N, Frisenda R and Castellanos-Gomez A 2020 Microheater actuators as a versatile platform for strain engineering in 2D materials *Nano Lett.* **20** 5339–45
[29] Di Giorgio C, Blundo E, Pettinari G, Felici M, Polimeni A and Bobba F 2021 Exceptional elasticity of microscale constrained MoS_2 domes *ACS Appl. Mater. Interfaces* **13** 48228–38
[30] Blundo E, Cappelluti E, Felici M, Pettinari G and Polimeni A 2021 Strain-tuning of the electronic, optical and vibrational properties of two-dimensional crystals *Appl. Phys. Rev.* **8** 021318
[31] Blundo E *et al* 2022 Strain-induced exciton hybridization in WS_2 monolayers unveiled by Zeeman-splitting measurements *Phys. Rev. Lett.* **129** 067402
[32] Di Giorgio C, Blundo E, Pettinari G, Felici M, Bobba F and Polimeni A 2022 Mechanical, elastic and adhesive properties of two-dimensional materials: from straining techniques to state-of-the-art local probe measurements *Adv. Mater. Interfaces* **9** 2102220
[33] Branny A, Kumar S, Proux R and Gerardot B D 2017 Deterministic strain-induced arrays of quantum emitters in a two-dimensional semiconductor *Nat. Commun.* **8** 15053
[34] Mak K F, Lee C, Hone J, Shan J and Heinz T F 2010 Atomically thin MoS_2: a new direct-gap semiconductor *Phys. Rev. Lett.* **105** 136805
[35] Splendiani A, Sun L, Zhang Y, Tianshu Li, Kim J, Chim C-Y, Galli G and Wang F 2010 Emerging photoluminescence in monolayer MoS_2 *Nano Lett.* **10** 1271–5
[36] Tonndorf P *et al* 2013 Photoluminescence emission and Raman response of monolayer MoS_2, $MoSe_2$ and WSe_2 *Opt. Express* **21** 4908–16
[37] Wang G, Chernikov A, Glazov M M, Heinz T F, Marie X, Amand T and Urbaszek B 2018 Colloquium: excitons in atomically thin transition metal dichalcogenides *Rev. Mod. Phys.* **90** 021001
[38] He X-F 1991 Excitons in anisotropic solids: the model of fractional-dimensional space *Phys. Rev.* B **43** 2063–9
[39] Blundo E, Felici M, Yildirim T, Pettinari G, Tedeschi D, Antonio Miriametro A, Liu B, Ma W, Lu Y and Polimeni A 2020 Evidence of the direct-to-indirect band gap transition in strained two-dimensional WS_2, MoS_2 and WSe_2 *Phys. Rev. Res.* **2** 012024
[40] Brown R H H and Twiss R Q 1956 Correlation between photons in two coherent beams of light *Nature* **177** 27–29
[41] Tonndorf P, Schmidt R Schneider R, Kern J, Buscema M, Steele G A, Castellanos-Gomez A, van der Zant H S J, de Vasconcellos S M and Bratschitsch R 2015 Single-photon emission from localized excitons in an atomically thin semiconductor *Optica* **2** 347–52
[42] Kumar S, Kaczmarczyk A and Gerardot B D 2015 Strain-induced spatial and spectral isolation of quantum emitters in mono-and bilayer WSe_2 *Nano Lett.* **15** 7567–73
[43] Palacios-Berraquero C *et al* 2016 Atomically thin quantum light-emitting diodes *Nat. Commun.* **7** 12978
[44] Cianci S *et al* 2023 Spatially controlled single photon emitters in hBN-capped WS_2 domes *Adv. Opt. Mater.* **11** 2202953
[45] Chakraborty C, Goodfellow K M and Nick Vamivakas A 2016 Localized emission from defects in $MoSe_2$ layers *Opt. Mater. Express* **6** 2081–7
[46] Branny A, Wang G, Kumar S, Robert C, Lassagne B, Marie X, Gerardot B D and Urbaszek B 2016 Discrete quantum dot like emitters in monolayer $MoSe_2$: spatial mapping, magneto-optics and charge tuning *Appl. Phys. Lett.* **108** 142101
[47] Leo Y, Deng M, Linda Zhang J, Borghardt S, Kardynal B, Vučković J and Heinz T F 2021 Site-controlled quantum emitters in monolayer $MoSe_2$ *Nano Lett.* **21** 2376–81

[48] Klein J et al 2019 Site-selectively generated photon emitters in monolayer MoS_2 via local helium ion irradiation *Nat. Commun.* **10** 2755
[49] Pucko K O et al 2022 Excitons and trions in WSSe monolayers *2D Mater.* **10** 015018
[50] Kern J et al 2016 Nanoscale positioning of single-photon emitters in atomically thin WSe_2 *Adv. Mater.* **28** 7101–5
[51] Palacios-Berraquero C, Kara D M, Montblanch A R-P, Barbone M, Latawiec P, Yoon D, Ott A K, Loncar M, Ferrari A C and Atatüre M 2017 Large-scale quantum-emitter arrays in atomically thin semiconductors *Nat. Commun.* **8** 15093
[52] Kim G et al 2022 High-density, localized quantum emitters in strained 2D semiconductors *ACS Nano* **16** 9651–9
[53] Gao T, von Helversen M, Antón-Solanas C, Schneider C and Heindel T 2023 Atomically-thin single-photon sources for quantum communication *npj 2D Mater. Appl.* **7** 4
[54] de Brito C S, Rabahi C R, Daldin Teodoro M, Franco D F, Nalin M, Barcelos I D and Gobato Y G 2022 Strain engineering of quantum confinement in WSe_2 on nano-roughness glass substrates *Appl. Phys. Lett.* **121** 070601
[55] Rosenberger M R, Kavir Dass C, Chuang H-J, Sivaram S V, McCreary K M, Hendrickson J R and Jonker B T 2019 Quantum calligraphy: writing single-photon emitters in a two-dimensional materials platform *ACS Nano* **13** 904–12
[56] So J-P et al 2021 Polarization control of deterministic single-photon emitters in monolayer WSe_2 *Nano Lett.* **21** 1546–54
[57] Wang Q, Maisch J, Tang F, Zhao D, Yang S, Joos R, Luca Portalupi S L, Michler P and Smet J H 2021 Highly polarized single photons from strain-induced quasi-1D localized excitons in WSe_2 *Nano Lett.* **21** 7175–82
[58] Linhart L, Paur M, Smejkal V, Burgdörfer J, Mueller T and Libisch F 2019 Localized intervalley defect excitons as single-photon emitters in WSe_2 *Phys. Rev. Lett.* **123** 146401
[59] Zhu Z Y, Cheng Y C and Schwingenschlögl U 2011 Giant spin-orbit-induced spin splitting in two-dimensional transition-metal dichalcogenide semiconductors *Phys. Rev.* B **84** 153402
[60] Xiao Di, Liu G-B, Feng W, Xu X and Yao W 2012 Coupled spin and valley physics in monolayers of MoS_2 and other group-VI dichalcogenides *Phys. Rev. Lett.* **108** 196802
[61] Molas M R et al 2019 Probing and manipulating valley coherence of dark excitons in monolayer WSe_2 *Phys. Rev. Lett.* **123** 096803
[62] Jie Zheng Y J et al 2019 Point defects and localized excitons in 2D WSe_2 *ACS Nano* **13** 6050–9
[63] Dang J et al 2020 Identifying defect-related quantum emitters in monolayer WSe_2 *npj 2D Mater. Appl.* **4** 2
[64] Ping Y and Smart T J 2021 Computational design of quantum defects in two-dimensional materials *Nat. Comput. Sci.* **1** 646–54
[65] Wang D, Han D, Li X-B, Xie S-Y, Chen N-K, Tian W Q Q, West D, Sun H-B and Zhang S B 2015 Determination of formation and ionization energies of charged defects in two-dimensional materials *Phys. Rev. Lett.* **114** 196801
[66] Komsa H-P, Berseneva N, Krasheninnikov A V and Nieminen R M 2014 Charged point defects in the flatland: accurate formation energy calculations in two-dimensional materials *Phys. Rev.* X **4** 031044
[67] Feng W, Galatas A, Sundararaman R, Rocca D and Ping Y 2017 First-principles engineering of charged defects for two-dimensional quantum technologies *Phys. Rev. Mater.* **1** 071001
[68] Smart T J, Wu F, Govoni M and Ping Y 2018 Fundamental principles for calculating charged defect ionization energies in ultrathin two-dimensional materials *Phys. Rev. Mater.* **2** 124002
[69] Zhu G-J, Yang J-H and Gong X-G 2020 Self-consistently determining structures of charged defects and defect ionization energies in low-dimensional semiconductors *Phys. Rev.* B **102** 035202
[70] Da Silva M C, Lorke M, Aradi B, Tabriz M F, Frauenheim T, Rubio A, Rocca D and Deák P 2021 Self-consistent potential correction for charged periodic systems *Phys. Rev. Lett.* **126** 076401
[71] Gupta S, Yang J-H and Yakobson B I 2018 Two-level quantum systems in two-dimensional materials for single photon emission *Nano Lett.* **19** 408–14
[72] Moon H, Bersin E, Chakraborty C, Lu A-Y, Grosso G, Kong J and Englund D 2020 Strain-correlated localized exciton energy in atomically thin semiconductors *ACS Photonics* **7** 1135–40
[73] Parto K, Azzam S I, Banerjee K and Moody G 2021 Defect and strain engineering of monolayer WSe_2 enables site-controlled single-photon emission up to 150 K *Nat. Commun.* **12** 3585
[74] Xu D D, Vong A F, Lebedev D, Ananth R, Wong A M, Brown P T, Hersam M C, Mirkin C A and Weiss E A 2023 Conversion of classical light emission from a nanoparticle-strained WSe_2 monolayer into quantum light emission via electron beam irradiation *Adv. Mater.* **35** 2208066
[75] Chirolli L, Prada E, Guinea F, Roldán R and San-Jose P 2019 Strain-induced bound states in transition-metal dichalcogenide bubbles *2D Mater.* **6** 025010
[76] Feng J, Qian X, Huang C-W and Li J 2012 Strain-engineered artificial atom as a broad-spectrum solar energy funnel *Nat. Photon.* **6** 866–72
[77] Shepard G D, Ajayi O A, Xiangzhi Li X Y Z, Hone J and Strauf S 2017 Nanobubble induced formation of quantum emitters in monolayer semiconductors *2D Mater.* **4** 021019
[78] Darlington T P et al 2020 Imaging strain-localized excitons in nanoscale bubbles of monolayer WSe_2 at room temperature *Nat. Nanotechnol.* **15** 854–60
[79] Carmesin C, Lorke M, Florian M, Erben D, Schulz A, Wehling T O and Jahnke F 2019 Quantum-dot-like states in molybdenum disulfide nanostructures due to the interplay of local surface wrinkling, strain and dielectric confinement *Nano Lett.* **19** 3182–6
[80] Mitterreiter E et al 2021 The role of chalcogen vacancies for atomic defect emission in MoS_2 *Nat. Commun.* **12** 3822
[81] Klein J et al 2021 Engineering the luminescence and generation of individual defect emitters in atomically thin MoS_2 *ACS Photonics* **8** 669–77
[82] Hötger A et al 2023 Spin-defect characteristics of single sulfur vacancies in monolayer MoS_2 *npj 2D Mater. Appl.* **7** 30
[83] Zhang Z et al 2022 Optically active chalcogen vacancies in monolayer semiconductors *Adv. Opt. Mater.* **10** 2201350
[84] Tedeschi D et al 2019 Controlled micro/nanodome formation in proton-irradiated bulk transition-metal dichalcogenides *Adv. Mater.* **31** 1903795
[85] Mazzucato S, Nardin D, Capizzi M, Polimeni A, Frova A, Seravalli L and Franchi S 2005 Defect passivation in strain engineered InAs/(InGa) as quantum dots *Mater. Sci. Eng.* C **25** 830–4
[86] Wang W, Jones L O, Chen J-S, Schatz G C and Ma X 2022 Utilizing ultraviolet photons to generate single-photon emitters in semiconductor monolayers *ACS Nano* **16** 21240–7
[87] Hötger A et al 2021 Gate-switchable arrays of quantum light emitters in contacted monolayer MoS_2 van der Waals heterodevices *Nano Lett.* **21** 1040–6
[88] Yu-Ming H, Iff O, Lundt N, Baumann V, Davanco M, Srinivasan K, Höfling S and Schneider C 2016 Cascaded emission of single photons from the biexciton in monolayered WSe_2 *Nat. Commun.* **7** 13409
[89] Giovannetti V, Lloyd S and Maccone L 2011 Advances in quantum metrology *Nat. Photon.* **5** 222–9

[90] Huang Z, Macchiavello C and Maccone L 2016 Usefulness of entanglement-assisted quantum metrology *Phys. Rev.* A **94** 012101
[91] Ioannou K and Solomos D 2015 Quantum radars: fundamental physical framework and practical aspects of an emerging defense technology *6th Int. Conf. IC-EpsMsO* pp 8–11
[92] Ma X, Fred Fung C-H and Lo H-K 2007 Quantum key distribution with entangled photon sources *Phys. Rev.* A **76** 012307
[93] Schimpf C, Reindl M, Huber D, Lehner B, Covre Da Silva S F, Manna S, Vyvlecka M, Walther P and Rastelli A 2021 Quantum cryptography with highly entangled photons from semiconductor quantum dots *Sci. Adv.* **7** eabe8905
[94] Vajner D A, Rickert L, Gao T, Kaymazlar K and Heindel T 2022 Quantum communication using semiconductor quantum dots *Adv. Quantum Technol.* **5** 2100116
[95] DiVincenzo D P 1995 Quantum computation *Science* **270** 255–61
[96] O'brien J L 2007 Optical quantum computing *Science* **318** 1567–70
[97] Iff O *et al* 2019 Strain-tunable single photon sources in WSe_2 monolayers *Nano Lett.* **19** 6931–6
[98] Kim H, Moon J S S, Noh G, Lee J and Kim J-H 2019 Position and frequency control of strain-induced quantum emitters in WSe_2 monolayers *Nano Lett.* **19** 7534–9
[99] Chakraborty C, Jungwirth N R, Fuchs G D and Nick Vamivakas A 2019 Electrical manipulation of the fine-structure splitting of WSe_2 quantum emitters *Phys. Rev.* B **99** 045308
[100] Brotons-Gisbert M, Branny A, Kumar S, Picard R Proux R, Gray M, Burch K S, Watanabe K, Taniguchi T and Gerardot B D 2019 Coulomb blockade in an atomically thin quantum dot coupled to a tunable Fermi reservoir *Nat. Nanotechnol.* **14** 442–6
[101] Chakraborty C, Qiu L, Konthasinghe K, Mukherjee A, Dhara S and Vamivakas N 2018 3d localized trions in monolayer WSe_2 in a charge tunable van der Waals heterostructure *Nano Lett.* **18** 2859–63
[102] Lenferink E J, LaMountain T, Stanev T K, Garvey E, Watanabe K, Taniguchi T and Stern N P 2022 Tunable emission from localized excitons deterministically positioned in monolayer p–n junctions *ACS Photonics* **9** 3067–74
[103] Oreszczuk K, Slawinska J, Rodek A, Potemski M, Skierbiszewski C and Kossacki P 2022 Hybrid electroluminescent devices composed of (In,Ga)N micro-LEDs and monolayers of transition metal dichalcogenides *Nanoscale* **14** 17271–6
[104] Geim A K and Grigorieva I V 2013 Van der Waals heterostructures *Nature* **499** 419–25
[105] Karni O *et al* 2019 Infrared interlayer exciton emission in MoS_2/WSe_2 heterostructures *Phys. Rev. Lett.* **123** 247402
[106] Rivera P *et al* 2015 Observation of long-lived interlayer excitons in monolayer $MoSe_2$–WSe_2 heterostructures *Nat. Commun.* **6** 6242
[107] Rivera P, Seyler K L, Yu H, Schaibley J R, Yan J, Mandrus D G, Yao W and Xu X 2016 Valley-polarized exciton dynamics in a 2D semiconductor heterostructure *Science* **351** 688–91
[108] Nagler P *et al* 2017 Interlayer exciton dynamics in a dichalcogenide monolayer heterostructure *2D Mater.* **4** 025112
[109] Miller B, Steinhoff A, Pano B, Klein J, Jahnke F, Holleitner A and Wurstbauer U 2017 Long-lived direct and indirect interlayer excitons in van der Waals heterostructures *Nano Lett.* **17** 5229–37
[110] Nayak P K *et al* 2017 Probing evolution of twist-angle-dependent interlayer excitons in $MoSe_2/WSe_2$ van der Waals heterostructures *ACS Nano* **11** 4041–50
[111] Rivera P, Yu H, Seyler K L, Wilson N P, Yao W and Xu X 2018 Interlayer valley excitons in heterobilayers of transition metal dichalcogenides *Nat. Nanotechnol.* **13** 1004–15
[112] Montblanch A R-P *et al* 2021 Confinement of long-lived interlayer excitons in WS_2/WSe_2 heterostructures *Commun. Phys.* **4** 119
[113] Shanks D N *et al* 2021 Nanoscale trapping of interlayer excitons in a 2D semiconductor heterostructure *Nano Lett.* **21** 5641–7
[114] Bai Y *et al* 2020 Excitons in strain-induced one-dimensional moiré potentials at transition metal dichalcogenide heterojunctions *Nat. Mater.* **19** 1068–73
[115] Brotons-Gisbert M, Baek H, Molina-Sánchez A, Campbell A, Scerri E, White D, Watanabe K, Taniguchi T, Bonato C and Gerardot B D 2020 Spin–layer locking of interlayer excitons trapped in moiré potentials *Nat. Mater.* **19** 630–6
[116] Seyler K L, Rivera P, Hongyi Y, Wilson N P, Ray E L, Mandrus D G, Yan J, Yao W and Xiaodong X 2019 Signatures of moiré-trapped valley excitons in $MoSe_2/WSe_2$ heterobilayers *Nature* **567** 66–70
[117] Baek H, Brotons-Gisbert M, Xian Koong Z X, Campbell A, Rambach M, Watanabe K, Taniguchi T and Gerardot B D 2020 Highly energy-tunable quantum light from moiré-trapped excitons *Sci. Adv.* **6** eaba8526
[118] Zunger A, Katzir A and Halperin A 1976 Optical properties of hexagonal boron nitride *Phys. Rev.* B **13** 5560
[119] Gao J, Li B, Tan J, Chow P, Lu T-M and Koratkar N 2016 Aging of transition metal dichalcogenide monolayers *ACS Nano* **10** 2628–35
[120] Kim A-R J G, Jeong H Y, Lee Z, Kang D J and Shin H S 2013 Growth of high-crystalline, single-layer hexagonal boron nitride on recyclable platinum foil *Nano Lett.* **13** 1834–9
[121] Dean C R *et al* 2010 Boron nitride substrates for high-quality graphene electronics *Nat. Nanotechnol.* **5** 722–6
[122] Ajayi O A *et al* 2017 Approaching the intrinsic photoluminescence linewidth in transition metal dichalcogenide monolayers *2D Mater.* **4** 031011
[123] Cadiz F *et al* 2017 Excitonic linewidth approaching the homogeneous limit in MoS_2-based van der Waals heterostructures *Phys. Rev.* X **7** 021026
[124] Man M K L, Deckoff-Jones S, Winchester A, Shi G, Gupta G, Mohite A D, Kar S, Kioupakis E, Talapatra S and Dani K M 2016 Protecting the properties of monolayer MoS_2 on silicon based substrates with an atomically thin buffer *Sci. Rep.* **6** 1–9
[125] Wang H, Taychatanapat T, Hsu A, Watanabe K, Taniguchi T, Jarillo-Herrero P and Palacios T 2011 BN/graphene/BN transistors for RF applications *IEEE Electron Device Lett.* **32** 1209–11
[126] Mahalu D D, Peisach M, Jaegermann W, Wold A and Tenne R 1990 Controlled photocorrosion of tungsten diselenide: influence of molecular oxygen *J. Phys. Chem.* **94** 8012–3
[127] Solomon G S, Flagg E B, Polyakov S V, Thomay T and Muller A 2012 Manipulating single photons from disparate quantum sources to be indistinguishable *J. Opt. Soc. Am.* B **29** 319–27
[128] Yu S, Sun Y-N, Liu W, Liu Z-D, Ke Z-J, Wang Y-T, Tang J-S, Li C-F and Guo G-C 2019 Realization of a causal-modeled delayed-choice experiment using single photons *Phys. Rev.* A **100** 012115
[129] White S J U *et al* 2020 Quantum random number generation using a hexagonal boron nitride single photon emitter *J. Opt.* **23** 01LT01
[130] Fournier C, Roux S, Watanabe K, Taniguchi T, Buil S, Barjon J, Hermier J-P and Delteil A 2023 Two-photon interference from a quantum emitter in hexagonal boron nitride *Phys. Rev. Appl.* **19** L041003
[131] Jungwirth N R, Calderon B, Yanxin J, Spencer M G, Flatté M E and Fuchs G D 2016 Temperature dependence of wavelength selectable zero-phonon emission from single defects in hexagonal boron nitride *Nano Lett.* **16** 6052–7

[132] Tran T T T, Elbadawi C, Totonjian D, Lobo C J, Grosso G, Moon H, Englund D R, Ford M J, Aharonovich I and Toth M 2016 Robust multicolor single photon emission from point defects in hexagonal boron nitride *ACS Nano* **10** 7331–8
[133] Bourrellier R, Meuret S, Tararan A, Stéphan O, Kociak M, Tizei L H G and Zobelli A 2016 Bright UV single photon emission at point defects in h-BN *Nano Lett.* **16** 4317–21
[134] Kianinia M, Tawfik S A, Regan B, Trong Tran T, Ford M J, Aharonovich I and Toth M 2017 Robust solid state quantum system operating at 800 K *CLEO: QELS_fundamental Science* (Optica Publishing Group) p JTu5A–24
[135] Hernández-Mínguez A, Lähnemann J, Nakhaie S, Lopes J M J and Santos P V 2018 Luminescent defects in a few-layer h-BN film grown by molecular beam epitaxy *Phys. Rev. Appl.* **10** 044031
[136] Chejanovsky N *et al* 2016 Structural attributes and photodynamics of visible spectrum quantum emitters in hexagonal boron nitride *Nano Lett.* **16** 7037–45
[137] Chejanovsky N *et al* 2021 Single-spin resonance in a van der Waals embedded paramagnetic defect *Nat. Mater.* **20** 1079–84
[138] Choi S, Trong Tran T T, Elbadawi C, Lobo C, Wang X, Juodkazis S, Seniutinas G, Toth M and Aharonovich I 2016 Engineering and localization of quantum emitters in large hexagonal boron nitride layers *ACS Appl. Mater. Interfaces* **8** 29642–8
[139] Qian C *et al* 2022 Unveiling the zero-phonon line of the boron vacancy center by cavity-enhanced emission *Nano Lett.* **22** 5137–42
[140] Zai-Quan X *et al* 2018 Single photon emission from plasma treated 2D hexagonal boron nitride *Nanoscale* **10** 7957–65
[141] Vogl T, Campbell G, Buchler B C, Lu Y and Koy Lam P K 2018 Fabrication and deterministic transfer of high-quality quantum emitters in hexagonal boron nitride *ACS Photonics* **5** 2305–12
[142] Fischer M *et al* 2021 Controlled generation of luminescent centers in hexagonal boron nitride by irradiation engineering *Sci. Adv.* **7** eabe7138
[143] Fournier C *et al* 2021 Position-controlled quantum emitters with reproducible emission wavelength in hexagonal boron nitride *Nat. Commun.* **12** 3779
[144] Duong H N M, Nguyen M A P, Kianinia M, Ohshima T, Abe H, Watanabe K, Taniguchi T, Edgar J H, Aharonovich I and Toth M 2018 Effects of high-energy electron irradiation on quantum emitters in hexagonal boron nitride *ACS Appl. Mater. Interfaces* **10** 24886–91
[145] Hou S, Birowosuto M D D, Umar S, Ange Anicet M A, Yingjie Tay R Y, Coquet P, Kang Tay B K, Wang H and Hang Tong Teo E 2017 Localized emission from laser-irradiated defects in 2D hexagonal boron nitride *2D Mater.* **5** 015010
[146] Vogl T, Doherty M W, Buchler B C, Lu Y and Koy Lam P K 2019 Atomic localization of quantum emitters in multilayer hexagonal boron nitride *Nanoscale* **11** 14362–71
[147] Breitweiser S A, Exarhos A L, Patel R N, Saouaf J, Porat B, Hopper D A and Bassett L C 2019 Efficient optical quantification of heterogeneous emitter ensembles *ACS Photonics* **7** 288–95
[148] Grosso G, Moon H, Lienhard B, Ali S, Efetov D K, Furchi M M, Jarillo-Herrero P, Ford M J, Aharonovich I and Englund D 2017 Tunable and high-purity room temperature single-photon emission from atomic defects in hexagonal boron nitride *Nat. Commun.* **8** 1–8
[149] Chejanovsky N, Kim Y, Zappe A, Stuhlhofer B, Taniguchi T, Watanabe K, Dasari D, Finkler A, Smet J H and Wrachtrup J 2017 Quantum light in curved low dimensional hexagonal boron nitride systems *Sci. Rep.* **7** 1–14
[150] Proscia N V, Shotan Z, Jayakumar H, Reddy P, Cohen C, Dollar M, Alkauskas A, Doherty M, Meriles C A and Menon V M 2018 Near-deterministic activation of room-temperature quantum emitters in hexagonal boron nitride *Optica* **5** 1128–34
[151] Chi Li, Mendelson N, Ritika R, Chen Y, Zai-Quan X, Toth M and Aharonovich I 2021 Scalable and deterministic fabrication of quantum emitter arrays from hexagonal boron nitride *Nano Lett.* **21** 3626–32
[152] Xu X, Martin Z O, Sychev D, Lagutchev A S, Chen Y P, Taniguchi T, Watanabe K, Shalaev V M and Boltasseva A 2021 Creating quantum emitters in hexagonal boron nitride deterministically on chip-compatible substrates *Nano Lett.* **21** 8182–9
[153] Ziegler J, Klaiss R, Blaikie A, Miller D, Horowitz V R and Alemán B J 2019 Deterministic quantum emitter formation in hexagonal boron nitride via controlled edge creation *Nano Lett.* **19** 2121–7
[154] Yim D, Yu M, Noh G, Lee J and Seo H 2020 Polarization and localization of single-photon emitters in hexagonal boron nitride wrinkles *ACS Appl. Mater. Interfaces* **12** 36362–9
[155] Mendelson N, Zai-Quan X, Trong Tran T, Kianinia M, Scott J, Bradac C, Aharonovich I and Toth M 2019 Engineering and tuning of quantum emitters in few-layer hexagonal boron nitride *ACS Nano* **13** 3132–40
[156] Stern H L *et al* 2019 Spectrally resolved photodynamics of individual emitters in large-area monolayers of hexagonal boron nitride *ACS Nano* **13** 4538–47
[157] Mendelson N *et al* 2021 Identifying carbon as the source of visible single-photon emission from hexagonal boron nitride *Nat. Mater.* **20** 321–8
[158] Weston L, Wickramaratne D, Mackoit M, Alkauskas A and Van de Walle C G 2018 Native point defects and impurities in hexagonal boron nitride *Phys. Rev.* B **97** 214104
[159] Sajid A, Reimers J R and Ford M J 2018 Defect states in hexagonal boron nitride: assignments of observed properties and prediction of properties relevant to quantum computation *Phys. Rev.* B **97** 064101
[160] Reimers J R, Sajid A, Kobayashi R and Ford M J 2018 Understanding and calibrating density-functional-theory calculations describing the energy and spectroscopy of defect sites in hexagonal boron nitride *J. Chem. Theory Comput.* **14** 1602–13
[161] Abdi M, Chou J-P, Gali A and Plenio M B 2018 Color centers in hexagonal boron nitride monolayers: a group theory and ab initio analysis *ACS Photonics* **5** 1967–76
[162] Korkmaz Y A, Bulutay C and Sevik C 2020 Defect states in monolayer hexagonal BN: a comparative DFT and DFT-1/2 study *Physica* B **584** 411959
[163] Reimers J R, Sajid A, Kobayashi R and Ford M J 2020 Convergence of defect energetics calculations *J. Phys. Chem.* C **124** 21178–83
[164] Gao S, Chen H-Y and Bernardi M 2021 Radiative properties of quantum emitters in boron nitride from excited state calculations and Bayesian analysis *npj Comput. Mater.* **7** 85
[165] Auburger P and Gali A 2021 Towards ab initio identification of paramagnetic substitutional carbon defects in hexagonal boron nitride acting as quantum bits *Phys. Rev.* B **104** 075410
[166] Jara C, Rauch T, Botti S, Marques M A L, Norambuena A, Raul Coto J E C-Aguila, Maze J R and Munoz F 2021 First-principles identification of single photon emitters based on carbon clusters in hexagonal boron nitride *J. Phys. Chem.* A **125** 1325–35
[167] Linderälv C, Wieczorek W and Erhart P 2021 Vibrational signatures for the identification of single-photon emitters in hexagonal boron nitride *Phys. Rev.* B **103** 115421
[168] Mackoit-Sinkevičienė M, Maciaszek M, Van de Walle C G and Alkauskas A 2019 Carbon dimer defect as a source of the 4.1 eV luminescence in hexagonal boron nitride *Appl. Phys. Lett.* **115** 212101

[169] Noh G, Choi D, Kim J-H, Dong-Gil I, Kim Y-H, Seo H and Lee J 2018 Stark tuning of single-photon emitters in hexagonal boron nitride *Nano Lett.* **18** 4710–5
[170] Xia Y, Li Q, Kim J, Bao W, Gong C, Yang S, Wang Y and Zhang X 2019 Room-temperature giant Stark effect of single photon emitter in van der Waals material *Nano Lett.* **19** 7100–5
[171] Nikolay N, Mendelson N, Sadzak N, Böhm F, Trong Tran T, Sontheimer B, Aharonovich I and Benson O 2019 Very large and reversible Stark-shift tuning of single emitters in layered hexagonal boron nitride *Phys. Rev. Appl.* **11** 041001
[172] Exarhos A L, Hopper D A, Grote R R, Alkauskas A and Bassett L C 2017 Optical signatures of quantum emitters in suspended hexagonal boron nitride *ACS Nano* **11** 3328–36
[173] Li X, Shepard G D, Cupo A, Camporeale N, Shayan K, Luo Y, Meunier V and Strauf S 2017 Nonmagnetic quantum emitters in boron nitride with ultranarrow and sideband-free emission spectra *ACS Nano* **11** 6652–60
[174] Abidi I H, Mendelson N, Trong Tran T T, Tyagi A, Zhuang M, Weng L-T, Özyilmaz B, Aharonovich I, Toth M and Luo Z 2019 Selective defect formation in hexagonal boron nitride *Adv. Opt. Mater.* **7** 1900397
[175] Stewart J C C *et al* 2021 Quantum emitter localization in layer-engineered hexagonal boron nitride *ACS Nano* **15** 13591–603
[176] Zai-Quan X, Mendelson N, Scott J A, Chi Li, Abidi I H, Liu H, Luo Z, Aharonovich I and Toth M 2020 Charge and energy transfer of quantum emitters in 2D heterostructures *2D Mater.* **7** 031001
[177] Sontheimer B, Braun M, Nikolay N, Sadzak N, Aharonovich I and Benson O 2017 Photodynamics of quantum emitters in hexagonal boron nitride revealed by low-temperature spectroscopy *Phys. Rev.* B **96** 121202
[178] Spokoyny B, Utzat H, Moon H, Grosso G, Englund D and Bawendi M G 2020 Effect of spectral diffusion on the coherence properties of a single quantum emitter in hexagonal boron nitride *J. Phys. Chem. Lett.* **11** 1330–5
[179] Trong Tran T T, Kianinia M, Nguyen M, Kim S, Xu Z-Q, Kubanek A, Toth M and Aharonovich I 2018 Resonant excitation of quantum emitters in hexagonal boron nitride *ACS Photonics* **5** 295–300
[180] Konthasinghe K, Chakraborty C, Mathur N, Qiu L, Mukherjee A, Fuchs G D and Nick Vamivakas A 2019 Rabi oscillations and resonance fluorescence from a single hexagonal boron nitride quantum emitter *Optica* **6** 542–8
[181] Akbari H, Lin W-H, Vest B, Jha P K and Atwater H A 2021 Temperature-dependent spectral emission of hexagonal boron nitride quantum emitters on conductive and dielectric substrates *Phys. Rev. Appl.* **15** 014036
[182] White S, Stewart C, Solntsev A S, Li C, Toth M, Kianinia M and Aharonovich I 2021 Phonon dephasing and spectral diffusion of quantum emitters in hexagonal boron nitride *Optica* **8** 1153–8
[183] Andreas Dietrich M B, Steiger E S, Antoniuk L, Toan Tran T, Nguyen M, Aharonovich I, Jelezko F and Kubanek A 2018 Observation of Fourier transform limited lines in hexagonal boron nitride *Phys. Rev.* B **98** 081414
[184] White S J U, My Hanh Duong N, Solntsev A S, Kim J-H, Kianinia M and Aharonovich I 2020 Optical repumping of resonantly excited quantum emitters in hexagonal boron nitride *Phys. Rev. Appl.* **14** 044017
[185] Andreas Dietrich M W D, Aharonovich I and Kubanek A 2020 Solid-state single photon source with Fourier transform limited lines at room temperature *Phys. Rev.* B **101** 081401
[186] Hoese M, Reddy P, Dietrich A, Koch M K, Fehler K G, Doherty M W and Kubanek A 2020 Mechanical decoupling of quantum emitters in hexagonal boron nitride from low-energy phonon modes *Sci. Adv.* **6** eaba6038
[187] Koperski M, Nogajewski K and Potemski M 2018 Single photon emitters in boron nitride: More than a supplementary material *Opt. Commun.* **411** 158–65
[188] Exarhos A L, Hopper D A, Patel R N, Doherty M W and Bassett L C 2019 Magnetic-field-dependent quantum emission in hexagonal boron nitride at room temperature *Nat. Commun.* **10** 222
[189] Wolfowicz F J H G, Anderson C P, Kanai S, Seo H, Gali A, Galli G and Awschalom D D 2021 Quantum guidelines for solid-state spin defects *Nat. Rev. Mater.* **6** 906–25
[190] Gottscholl A *et al* 2020 Initialization and read-out of intrinsic spin defects in a van der Waals crystal at room temperature *Nat. Mater.* **19** 540–5
[191] Zhao M *et al* 2022 Excited-state optically detected magnetic resonance of spin defects in hexagonal boron nitride *Phys. Rev. Lett.* **128** 216402
[192] Korkut H and Sarpkaya İ 2022 Controlling the photoluminescence of quantum emitters in hexagonal boron nitride by external magnetic fields *2D Mater.* **10** 015004
[193] Stern H L *et al* 2022 Room-temperature optically detected magnetic resonance of single defects in hexagonal boron nitride *Nat. Commun.* **13** 618
[194] Mills Purcell E 1995 Spontaneous emission probabilities at radio frequencies *Confined Electrons and Photons: New Physics and Applications* (*NATO ASI Series* vol 340) (Springer) p 839
[195] Cai T, Dutta S, Aghaeimeibodi S, Yang Z, Nah S, Fourkas J T and Waks E 2017 Coupling emission from single localized defects in two-dimensional semiconductor to surface plasmon polaritons *Nano Lett.* **17** 6564–8
[196] Tripathi L N, Iff O, Betzold S, Dusanowski Ł, Emmerling M, Moon K, Jin Lee Y, Kwon S-H, Höfling S and Schneider C 2018 Spontaneous emission enhancement in strain-induced WSe_2 monolayer-based quantum light sources on metallic surfaces *ACS Photonics* **5** 1919–26
[197] Iff O, Lundt N, Betzold S, Tripathi L N, Emmerling M, Tongay S, Jin Lee Y, Kwon S-H, Höfling S and Schneider C 2018 Deterministic coupling of quantum emitters in WSe_2 monolayers to plasmonic nanocavities *Opt. Express* **26** 25944–51
[198] Cai T, Kim J-H, Yang Z, Dutta S, Aghaeimeibodi S and Waks E 2018 Radiative enhancement of single quantum emitters in WSe_2 monolayers using site-controlled metallic nanopillars *ACS Photonics* **5** 3466–71
[199] Luo Y, Shepard G D, Ardelean J V, Rhodes D A, Kim B, Barmak K, Hone J C and Strauf S 2018 Deterministic coupling of site-controlled quantum emitters in monolayer WSe_2 to plasmonic nanocavities *Nat. Nanotechnol.* **13** 1137–42
[200] Luo Y, Liu N, Xiangzhi Li, Hone J C and Strauf S 2019 Single photon emission in WSe_2 up 160 K by quantum yield control *2D Mater.* **6** 035017
[201] Peng L, Chan H, Choo P, Odom T W, Sankaranarayanan S K R S and Xuedan M 2020 Creation of single-photon emitters in WSe_2 monolayers using nanometer-sized gold tips *Nano Lett.* **20** 5866–72
[202] Iff O *et al* 2021 Purcell-enhanced single photon source based on a deterministically placed WSe_2 monolayer quantum dot in a circular Bragg grating cavity *Nano Lett.* **21** 4715–20
[203] Sortino L, Zotev P G, Phillips C L, Brash A J, Cambiasso J, Marensi A M F E, Maier S A, Sapienza R and Tartakovskii A I 2021 Bright single photon emitters with enhanced quantum efficiency in a two-dimensional semiconductor coupled with dielectric nano-antennas *Nat. Commun.* **12** 6063
[204] Azzam S I, Parto K and Moody G 2023 Purcell enhancement and polarization control of single-photon emitters in monolayer WSe_2 using dielectric nanoantennas *Nanophotonics* **12** 477–84

[205] Flatten L C, Weng L, Branny A, Sam Johnson P R D, Trichet A A P, Gerardot B D and Smith J M 2018 Microcavity enhanced single photon emission from two-dimensional WSe_2 *Appl. Phys. Lett.* **112** 191105
[206] Drawer J-C *et al* 2023 Monolayer-based single-photon source in a liquid-helium-free open cavity featuring 65% brightness and quantum coherence *Nano Lett.* **23** 8683–9
[207] Mäx Blauth M J, Vest G, Hartwig O, Prechtl M, Cerne J, Finley J J and Kaniber M 2018 Coupling single photons from discrete quantum emitters in WSe_2 to lithographically defined plasmonic slot waveguides *Nano Lett.* **18** 6812–9
[208] Peyskens F, Chakraborty C, Muneeb M, Van Thourhout D and Englund D 2019 Integration of single photon emitters in 2D layered materials with a silicon nitride photonic chip *Nat. Commun.* **10** 4435
[209] White D, Branny A, Chapman R J, Picard R, Brotons-Gisbert M, Boes A, Peruzzo A, Bonato C and Gerardot B D 2019 Atomically-thin quantum dots integrated with lithium niobate photonic chips *Opt. Mater. Express* **9** 441–8
[210] Errando-Herranz C *et al* 2021 Resonance fluorescence from waveguide-coupled, strain-localized, two-dimensional quantum emitters *ACS Photonics* **8** 1069–76
[211] Ma Y, Zhao H, Liu N, Gao Z, Sepehr Mohajerani S S, Xiao L, Hone J, Feng L and Strauf S 2022 On-chip spin-orbit locking of quantum emitters in 2D materials for chiral emission *Optica* **9** 953–8
[212] Kim S, Fröch J E, Christian J, Straw M, Bishop J, Totonjian D, Watanabe K, Taniguchi T, Toth M and Aharonovich I 2018 Photonic crystal cavities from hexagonal boron nitride *Nat. Commun.* **9** 2623
[213] Fröch J E, Spencer L P, Kianinia M, Totonjian D D, Nguyen M, Gottscholl A, Dyakonov V, Toth M, Kim S and Aharonovich I 2021 Coupling spin defects in hexagonal boron nitride to monolithic bullseye cavities *Nano Lett.* **21** 6549–55
[214] Fröch J E, Li C, Chen Y, Toth M, Kianinia M, Kim S and Aharonovich I 2022 Purcell enhancement of a cavity-coupled emitter in hexagonal boron nitride *Small* **18** 2104805
[215] Trong Tran T T, Wang D, Xu Z-Q, Yang A, Toth M, Odom T W and Aharonovich I 2017 Deterministic coupling of quantum emitters in 2D materials to plasmonic nanocavity arrays *Nano Lett.* **17** 2634–9
[216] Nguyen M, Kim S, Trong Tran T, Zai-Quan X, Kianinia M, Toth M and Aharonovich I 2018 Nanoassembly of quantum emitters in hexagonal boron nitride and gold nanospheres *Nanoscale* **10** 2267–74
[217] Proscia N V, Collison R J, Meriles C A and Menon V M 2019 Coupling of deterministically activated quantum emitters in hexagonal boron nitride to plasmonic surface lattice resonances *Nanophotonics* **8** 2057–64
[218] Mendelson N *et al* 2022 Coupling spin defects in a layered material to nanoscale plasmonic cavities *Adv. Mater.* **34** 2106046
[219] Gao X *et al* 2021 High-contrast plasmonic-enhanced shallow spin defects in hexagonal boron nitride for quantum sensing *Nano Lett.* **21** 7708–14
[220] Kim S, My Hanh Duong N, Nguyen M, Lu T-J, Kianinia M, Mendelson N, Solntsev A, Bradac C, Englund D R and Aharonovich I 2019 Integrated on chip platform with quantum emitters in layered materials *Adv. Opt. Mater.* **7** 1901132
[221] Li C, Fröch J E, Nonahal M, Tran T N, Toth M, Kim S and Aharonovich I 2021 Integration of hBN quantum emitters in monolithically fabricated waveguides *ACS Photonics* **8** 2966–72
[222] Parto K, Azzam S I, Lewis N, Patel S D, Umezawa S, Watanabe K, Taniguchi T and Moody G 2022 Cavity-enhanced 2D material quantum emitters deterministically integrated with silicon nitride microresonators *Nano Lett.* **22** 9748–56
[223] Vogl T, Lecamwasam R, Buchler B C, Lu Y and Koy Lam P K 2019 Compact cavity-enhanced single-photon generation with hexagonal boron nitride *ACS Photonics* **6** 1955–62
[224] Fröch J E, Kim S, Mendelson N, Kianinia M, Toth M and Aharonovich I 2020 Coupling hexagonal boron nitride quantum emitters to photonic crystal cavities *ACS Nano* **14** 7085–91
[225] Proscia N V, Jayakumar H, Xiaochen G, Lopez-Morales G, Shotan Z, Zhou W, Meriles C A and Menon V M 2020 Microcavity-coupled emitters in hexagonal boron nitride *Nanophotonics* **9** 2937–44
[226] Häußler S, Bayer G, Waltrich R, Mendelson N, Li C, Hunger D, Aharonovich I and Kubanek A 2021 Tunable fiber-cavity enhanced photon emission from defect centers in hBN *Adv. Opt. Mater.* **9** 2002218
[227] Patane A, Levine A, Polimeni A, Laurence Eaves P C M, Henini M and Hill G 2000 Carrier thermalization within a disordered ensemble of self-assembled quantum dots *Phys. Rev.* B **62** 11084